

CASE FILE
COPY

N 68 36 020
NASA CR-66667

METALLOGRAPHIC AND FRACTOGRAPHIC EXAMINATION

OF 7079 ALUMINUM ALLOY TEST SPECIMENS

By R. R. Boyer

and

J. C. McMillan

Distribution of this report is provided in the interest of information exchange. Responsibility for the contents resides in the author or organization that prepared it.

SEPTEMBER 1968

THE BOEING COMPANY

Renton, Washington

NATIONAL AERONAUTICS AND SPACE ADMINISTRATION

**METALLOGRAPHIC AND FRACTOGRAPHIC EXAMINATION
OF 7079 ALUMINUM ALLOY TEST SPECIMENS**

**By R. R. Boyer
and
J. C. McMillan**

**Distribution of this report is provided in the interest of
information exchange. Responsibility for the contents
resides in the author or organization that prepared it.**

**Prepared under Contract No. NAS 1-6474
by
THE BOEING COMPANY
Renton, Washington
for
NATIONAL AERONAUTICS AND SPACE ADMINISTRATION**

METALLOGRAPHIC AND FRACTOGRAPHIC EXAMINATION OF 7079 ALUMINUM ALLOY TEST SPECIMENS

By R. R. Boyer
and
J. C. McMillian

SUMMARY

This report summarizes the results of a metallographic and fractographic analysis of 7079 aluminum alloy test specimens tested under a separate task of this contract and reported in NASA CR-996. The examination was conducted as a function of specimen thickness and material heat treatment. The microstructural details and distribution of intermetallic particles were typical of wrought-7000-series aluminum alloys and were uniform through the thickness except for the thickest (0.630-inch) material tested. In this case, incomplete recrystallization was observed in the center of the plate.

Examination of the fractured test specimens showed that some of the apparent data anomalies could be explained in terms of the microstructural details. In particular, transverse splitting resulted in unexpectedly high-fracture-toughness values because of crack-tip blunting. Changes in fatigue-crack-propagation rate as a function of test environment were often accompanied by different fractographic appearances in the underaged and peak-aged condition. The tendency for transverse splitting was enhanced by underaging and by testing at low temperatures.

INTRODUCTION

The objective of the program was to conduct metallographic and fractographic examinations on failed specimens of 7079 aluminum alloy to determine the effects of microstructure and intermetallic particles on its fatigue crack propagation rate, residual strength, and fracture toughness. The specimens that were examined are those obtained by the tests reported in NASA Contractor Report CR-996.

The purpose of the work described in this report was:

- (1) To characterize the microscopic and submicroscopic structural details of the 7079 aluminum alloy to aid in understanding its fracture behavior.
- (2) To examine selected test specimens in an attempt to explain certain data anomalies and to document interesting or unusual fracture features.

SYMBOLS

G. P. zones	submicroscopic coherent precipitate particles
K	maximum-cyclic-stress-intensity factor ksi $\sqrt{\text{in.}}$
K _C	plane-stress critical-stress-intensity factor, ksi $\sqrt{\text{in.}}$
K _{Ic}	plane-strain critical-stress-intensity factor, ksi $\sqrt{\text{in.}}$
K _{Ii}	initial applied plane-strain stress-intensity level, ksi $\sqrt{\text{in.}}$
M	stable, incoherent MgZn ₂ precipitate particles
M'	metastable, semicoherent transition phase
R	ratio of minimum to maximum fatigue-cyclic-stress levels
W/A	precracked Charpy impact energy over net area of precracked Charpy specimen, in. -lb/in. ²
2a	fatigue crack length, in.

RESULTS AND DISCUSSION

Characterization of Materials

A detailed microstructural analysis of the 7079 aluminum alloy as a function of heat-treat condition and specimen thickness was performed using optical and electron metallography.















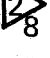
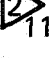
Optical metallography.—The optical metallography phase of this program had the following objectives:

- (1) To determine the characteristic grain size and shape as a function of material thickness
- (2) To characterize the size, shape, and identity of the intermetallic phases present
- (3) To characterize the occurrence and distribution of fine-scale chromium and manganese phases.

The characteristic grain size and shape are shown in three-dimensional-composite photomicrographs in figures 1 through 5 and 7 through 11. Table I lists the materials and conditions from which the three-dimensional composites were prepared.

TABLE I

TABULATION OF THREE-DIMENSIONAL COMPOSITE PHOTOMICROGRAPHS

Thickness	0.160 in.		0.250 in.			0.500 in.		0.630 in.	
Condition 	I	II	I	II	III	I	II	I	II
Magnification	86.5X	86.5X	86.5X	86.5X	440X	86.5X	86.5X	86.5X	86.5X
<u>Heat treatment</u>									
Underaged									
Peak Aged (T6)									
Overaged									



Conditions:

- I Etched to define intermetallics 10 sec in a solution of 0.5 percent HF in H₂O
- II Etched 1 min 30 sec in 1 part Keller's etchant in 3 parts H₂O
- III Etched 30 sec in 1 part Keller's etchant in 3 parts H₂O



Numbers designate the figure number of the photomicrograph.



Composites were prepared from sections near the surface and at midthickness of this specimen.

The material, with thicknesses of 0.160, 0.250, and 0.500 inch, exhibited the expected general grain structure characterized by elongated grains parallel to the rolling plane (figures 1, 2, and 3). Grain size, intermetallic distributions, and etching response were consistent throughout the thickness. Etching streaks parallel to the rolling plane in the lightly etched transverse sections are due to bands of small chromium and manganese intermetallics. These bands occur in all 7000-series aluminum alloys that contain these two elements. The bands are uniformly distributed throughout all of the 7079 aluminum alloy and there is no indication that their presence would have any effect on the mechanical or fracture test results.

Microstructure of the 0.630-inch-thick material (figures 4 and 5) varied through the thickness. The section taken near the surface shows a higher degree of recrystallization than the midthickness section. The heavily etched streaks in the short transverse plane of the midthickness section are bands where only the polygonization stage of recrystallization has been achieved. In thick material it is difficult to produce uniform deformation through the thickness. In this case, deformation at midthickness was insufficient to cause complete recrystallization. This unrecrystallized material would be expected to have fracture properties somewhat different from the surrounding recrystallized material. By comparing figure 5 with figures 1, 2, and 3, it can be seen that the grain size in the rolling plane is substantially larger for the thicker material at both locations. The degree of recrystallization was less for the thicker material even at the surface where the degree of deformation was greatest.

The exact significance of the difference in microstructure between the thickest material and the three thinner gages cannot be assessed. However in those tests reported in NASA CR-996 where the mechanical properties of the thickest material did not follow the apparent thickness trends, this microstructural variation must be considered in analyzing the results. A through-the-thickness composite comparing the microstructure of the 0.25-inch and 0.63-inch material as a function of thickness is shown in figure 6.

The effect of aging on microstructure was examined in the 0.25-inch-thick material and the results are shown in figures 2, 7, 8, 9, 10, and 11. No effect of aging is apparent in the very lightly etched specimens; however, it can be seen that increased aging greatly increases the etching response when more heavily etched. This was expected since increased precipitation results in increased chemical activity when the etchant is applied. Compare figures 9, 10, and 11 and observe that the definition of grain boundaries increases with aging time because of increased grain boundary precipitation and that some grains in the overaged specimen show a very heavy etching response. This difference in etching response from grain to grain is due to a lack of complete recrystallization and generally increases with the degree of aging. The fact that the 0.63-inch material showed this banding at midthickness in the underaged condition indicates that a smaller amount of the material had recrystallized.

The large intermetallics are often surrounded by regions of light etching response. Precipitation in close proximity to large intermetallics may not occur if: (a) the large particles act as sinks for vacancies; (b) solute depletion results from the formation of complex, multiphased compounds in association with the large intermetallics; or (c) the composition changes in the region of the intermetallics, which alters the reaction kinetics. A difficulty in nucleation appears to be the most probable cause, but the other effects probably play a part. This effect is normally observed in 7000-series aluminum alloys and should have no appreciable effect on the mechanical or fracture properties.

Figure 12 shows the intermetallics in high-magnification (1000X) detail. The intermetallics often contain iron and may be of the type Al_7Cu_2Fe . Another large intermetallic observed contains silicon in the form of Mg_2Si . The precipitate-depleted zone associated with the particles can be observed, but is not particularly pronounced. The zone often occurs in a band parallel to the rolling plane. The appearance and occurrence of intermetallics is typical for this type of alloy. Substantial differences in the quantity of intermetallics observed would cause differences in fracture behavior. The occurrence of intermetallics in these alloys is relatively uniform and should not significantly affect the test results.

Intergranular cracking parallel to the rolling plane was observed near the edges of the as-received 0.63-inch material. This type of cracking occurs in the vicinity of sheared edges in plate material. This material was apparently sheared by the producer. Intergranular cracks were not observed on test specimens prior to testing and there was no evidence that their presence on as-received stock in any way affected the test results.

Transmission electron microscopy.—The submicroscopic structural detail was examined using transmission electron microscopy techniques. Of primary interest were the changes in precipitate size and morphology as a function of aging time and temperature. Thin foils were prepared from specimens solution treated and quenched, and solution treated, quenched, and aged. Aging was accomplished at room temperature, 250°F, and 290°F for times ranging from 10 minutes to 10 days.

No precipitation was evident in the solution-treated, or solution-treated and room-temperature-aged specimens (figure 13), although some probably occurred during room-temperature aging as a slight increase in hardness was observed. Spherical G.P. zones were observed after a 10-minute age at elevated temperature and subsequent aging coarsened the particles (figures 14 and 15). No tendency for platelet formation was observed, and the spherical shape persisted throughout the aging sequence. No coherency strains were observed, but it is believed that the particles were originally the coherent G.P. zones and, with aging, lost coherency to form the M' and possibly the equilibrium (stable) M phase. Changes in the fracture and fatigue properties as a function of aging would be expected to be associated with the transitions from coherent to semicoherent to incoherent particles. These changes would be associated with the manner in which dislocations overcome obstacles to their motion. While the particles are coherent, passage of a dislocation through the coherent particle is possible. Once a dislocation has passed through the particle, the passage of additional dislocations through the particle on the same plane is favored, giving rise to coplanar arrays of dislocations and possible stress concentrations at pileups along grain boundaries. When the particles become incoherent, dislocation must circumvent the particles, and more tangled dislocation arrays result.

Analysis of Selected 7079 Aluminum Alloy Specimens

Selected test specimens of 7079 aluminum alloy were examined in an attempt to explain certain data anomalies, to further document interesting or unusual fracture features, and to characterize fatigue-crack-fracture topography. Optical and electron fractography and optical metallography were used in the examination. All specimen numbers and test data are those reported in "Fatigue-Crack-Propagation and Fracture-Toughness Characteristics of 7079 Aluminum-Alloy Sheets and Plates in Three Aged Conditions" by S. H. Smith, T. R. Porter, and W. D. Sump, NASA CR-996, dated February 1968.

Specimens 6U-11, 6P-11, and 6O-11.—In these surface-flawed specimens, the peak-aged material exhibited the highest toughness value. This was contrary to the expected behavior and did not correlate with data from the center-cracked-panel tests. The reported data are summarized in table II.

TABLE II
SUMMARY OF TOUGHNESS VALUES

Spec. no.	Grain direction	Heat treatment condition	$K_{IC}(\text{ksi}\sqrt{\text{in.}})$
6U-11	Longitudinal	Underaged	49.2
6P-11	Longitudinal	Peak (T6)	53.3
6O-11	Longitudinal	Overaged	44.6

Results: A photograph of the fractures is shown in figure 16. A tendency for transverse splitting or delamination is apparent in both the underaged and peak-strength specimens. Note particularly the deep transverse split near the tip of the fatigue zone in the peak-strength specimen. By contrast, no delaminations are observed on the overaged specimen.

Metallurgical sections through the specimen show in profile the machined notch, the fatigue zone, and the rapid-fracture zone, figure 17. The rapid-fracture zone of the underaged and peak-strength specimens is very serrated and lies along a plane approximately 45° to the tensile axis. The deep split in the peak-strength specimen is also readily apparent. The rapid-fracture zone of the overaged specimen, in addition to not showing serrations, is nearly normal to the tensile axis except for a small shear lip at the outside edge. The difference in microstructure through the thickness of this specimen is apparent in these micrographs (particularly the overaged specimen). The fracture features do not appear to correlate with this microstructural variation.

Conclusions: The high toughness of the peak-aged specimen was due to crack-tip blunting caused by the deep transverse split near the end of the fatigue crack. The serrated appearance of both the underaged and peak-strength specimens indicates some crack-tip blunting because of the delaminations that occurred across each specimen. Since this tendency for delamination is characteristic of the underaged and peak-aged materials, these toughness values are representative for tests in which the crack propagates through the thickness. Scatter in results could be large, with the actual value depending on the amount and the extent of the delamination encountered in each test. There was no evidence that the microstructural variations from surface to midthickness influenced the toughness values.

Specimens 6U-12, 6P-12, and 6O-12.—The surface-flaw-crack-growth rate data showed the overaged 7079 aluminum alloy produced the slowest, and the peak-aged material the fastest fatigue-crack-growth rates. The reported data are shown in table III.

TABLE III
SUMMARY OF FATIGUE DATA

Spec. no.	Gross area stress, ksi	K_{II}	Approximate cycles to failure
6U-12	43.49	45% of K_{IC}	3800
6P-12	47.11	45% of K_{IC}	1900
6O-12	39.43	45% of K_{IC}	4800

Results: The specimens are shown in figure 18. The underaged specimen presented an unusual appearance as shown in figure 19. The stress levels chosen for these tests were based upon the K_{IC} values obtained on other surface-flawed specimens. As was shown with specimens 6U-11, 6P-11, and 6O-11, the high apparent toughness of the peak strength material was due to crack-tip blunting at transverse delaminations, but the fatigue crack regions (figure 17) do not show delaminations. For this case, it appears that fatigue-crack-growth rates are more dependent upon K_{II} than on the ratio K_{II}/K_{IC} .

Conclusions: The effect of delamination on toughness was not anticipated when establishing the fatigue-test stress levels. The cycles-to-failure data reflect the influence of the actual cyclic stress value and do not give an indication of behavior under the same K_{II} conditions. In this case, a more meaningful comparison would have been achieved by using the same gross area stress for all three heat-treatment conditions.

Specimens 5U-3L, 5P-3L, and 5O-3L.—In general, the toughness of the underaged material was higher than the toughness of the overaged material. In this set of specimens, there was an apparent reversal of the behavior as measured by K_{IC} values. The reported data are summarized in table IV.

TABLE IV
SUMMARY OF TOUGHNESS VALUES

Spec. no.	Grain direction	Heat treatment condition	Width, inches	K_{IC} (ksi $\sqrt{\text{in.}}$)
5U-3L	Longitudinal	Underaged	8	55.3
5P-3L	Longitudinal	Peak (T6)	8	45.2
5O-3L	Longitudinal	Overaged	8	62.0

Results: A photograph of the fractures is shown in figure 20. The appearance of the fatigue zones was typical for the respective heat-treatment conditions, but the unusual appearance of the fatigue zones on the underaged and peak-aged materials have not been explained. This unusual fracture appearance was characterized by deviations from the general fracture plane. Compare 5U-3L and 5P-3L with 5O-3L in figure 20. These deviations increase with increasing stress intensity level and show some of the features expected in the development of shear lips except for their irregular nature. Overaging appears to provide a more homogeneous material as reflected in the uniform appearance of the fatigue zone of 5O-3L in figure 20.

The fatigue-to-fast-fracture transition was examined on these specimens in each heat-treat condition to determine if a difference could be observed fractographically. No difference was observed between the underaged and overaged materials. This is not surprising, however, as the difference was only about $5\sqrt{\text{ksi}}$ in. Figure 21 (from the underaged specimen) is typical of the interface for both conditions.

A difference was observed in the specimen heat treated to peak strength, however. The fatigue crack was propagating mostly by dimple rupture at this crack length, and there was no sharp transition observable from fatigue to fast fracture.

Conclusions: No metallurgical reason for the toughness anomaly was determined. The unusual fracture appearance of the fatigue zone in the underaged and peak-strength case appears to be related to microstructural inhomogeneties that can be removed by additional aging.

Fatigue fracture characterization.—A series of center-notched panels was examined to characterize the fatigue-crack-growth behavior as a function of heat treatment and test environment. The specimens examined and the test conditions employed are tabulated in table V.

TABLE V
SUMMARY OF FATIGUE TEST SPECIMENS AND TEST CONDITIONS

Specimen no.	Panel size, inches	Thickness, inches	Environment	R
2U-1L	12 by 36	0.25	Dry air	0.05
2P-1L	12 by 36	0.25	Dry air	0.05
2O-1L	12 by 36	0.25	Dry air	0.05
2U-1T	12 by 36	0.25	Dry air	0.67
2P-1T	12 by 36	0.25	Dry air	0.67
2O-1T	12 by 36	0.25	Dry air	0.67
2U-2T	12 by 36	0.25	Distilled H ₂ O	0.67
2P-2T	12 by 36	0.25	Distilled H ₂ O	0.67
2O-2T	12 by 36	0.25	Distilled H ₂ O	0.67
2U-2L	12 by 36	0.25	LN ₂ (-65°F)	0.05
2P-2L	12 by 36	0.25	LN ₂ (-65°F)	0.05
2O-2L	12 by 36	0.25	LN ₂ (-65°F)	0.05
6U-1T	12 by 36	0.63	Dry air	0.67
6P-1T	12 by 36	0.63	Dry air	0.67
6O-1T	12 by 36	0.63	Dry air	0.67
6U-2T	12 by 36	0.63	Distilled H ₂ O	0.67
6P-2T	12 by 36	0.63	Distilled H ₂ O	0.67
6O-2T	12 by 36	0.63	Distilled H ₂ O	0.67

Results: The 0.25-inch-thick specimens were examined at crack lengths (2a) of 0.75 (initiation), 0.85, 1.20, 1.60, 2.00, 3.00, and 3.50 inches (transition from fatigue to fast fracture). The 0.63-inch-thick specimens shown in figure 22 were examined at crack lengths (2a) of 1.0, 1.5, 2.25, and 3.25 inches. A systematic variation in fracture topography is apparent when comparing specimens tested in dry air with specimens tested in distilled water and with the remaining test conditions constant. These variations are illustrated in figures 23, 24, and 25 for the underaged, T6, and overaged conditions respectively. Note that all magnifications are the same and that the crack lengths and stress conditions are identical for each fracture area pictured.

Comparing figures 23a, 24a, and 25a (dry-air test environment), it is apparent that the prevailing crack-propagation mechanism is a ductile striation formation for all three aging conditions. It is also apparent that the striation spacing is smaller on the overaged specimen. By contrast, figures 23b and 24b (distilled-water environment) show examples of more brittle fractures, which are commonly termed brittle striations. These brittle striations often occur in 7000-series aluminum alloys when growth rates are accelerated by environmental effects. In the overaged condition, figure 25b, the specimen tested in the wet environment does not show the brittle striations, and only ductile striations are present. An additional comparison for peak-aged and overaged conditions is shown in figures 26 and 27 for the 0.63-inch material tested under both environmental conditions. The test results showed that the overaged specimens tested in the dry-air and distilled-water environments had slower growth rates than comparative specimens in the underaged or T6 conditions. It is also apparent that fatigue-crack-growth rates are noticeably increased in the aqueous environment for all three heat-treatment conditions. However, the wet-environment growth rate for the overaged material is approximately the same as dry-environment growth rates for the underaged and T6 conditions.

A change in R value ($R = 0.67$ to $R = 0.05$) for the dry-air condition changed the fracture appearance only by changes in striation spacing for the same crack length and an earlier onset of ductile tearing when $R = 0.05$. The striation spacings for the two R values at the same crack length are compared in figure 28a and b.

Testing at -65°F slowed the fatigue-crack-growth rates slightly. The striations were generally ill defined for specimens tested at this low temperature, figure 29. This observation was general for all heat-treat conditions. The reason for this behavior is not clearly understood, but may be related to the formation of a surface oxide during test. An analogous situation occurs when testing in vacuum where no striations are observed under high-vacuum conditions, but well-defined striations may be observed as atmospheric pressures are approached.

Conclusions: Both the underaged and peak-aged materials show a strong effect of a wet environment on crack growth rate evidenced by a change in fracture mode from ductile to brittle striations. The overaged material shows less environmental effect, and the fracture mode is predominantly ductile striation formation in both environments. The effect of reducing the R value of 0.67 to 0.05 is to increase the cracking rate as indicated by larger striation spacings for the same crack length and the earlier onset of ductile tearing modes. The low-temperature environment also changes the fracture appearance as compared to the dry-air case in that the striations are not well developed. This may be the result of differences in the surface oxide characteristics.

Specimens 5U-1L, 5P-1L, 5O-1L, 5U-2L, 5P-2L, and 5O-2L.—Delamination occurred on a number of specimens. These six specimens were examined to document this behavior.

Results: The fractured specimens are shown in figure 30. The -1L specimens were fracture tested at room temperature while the -2L series was tested at -65°F. Delamination or transverse splitting was particularly pronounced on the underaged and peak-aged specimens. Low temperatures accentuated this feature and the overaged specimen also experienced transverse splitting. The delamination is most extensive at the ends and decreases toward the centers of the specimens. The extent of the delaminations at the ends of the specimens is shown in figure 31. Sections through the material show this cracking to be intergranular in nature. For comparison, sections taken 1 inch from the end of the overaged specimen tested at room temperature and underaged specimen tested at -65°F are shown in figure 32.

Conclusions: These short transverse delaminations are intergranular indicating that the material cannot sustain high stresses in the short transverse direction without cracking along grain boundaries. The tendency toward delamination is enhanced by testing at low temperatures. Overaging reduces the tendency of the material to delaminate.

Specimens CNL-1U, CNL-1P, CNL-1O.—Very high toughness values were obtained for specimens CNL-1O and CNL-1U. The reported data are summarized in table VI.

TABLE VI
SUMMARY OF TOUGHNESS VALUES

Spec. no.	Width, inches	Heat treatment	K_{IC} (ksi $\sqrt{\text{in.}}$)
CNL-1U	36	Underaged	198
CNL-1P	36	Peak (T6)	96.6
CNL-1O	36	Overaged	170.4

Results: Fracture profiles for these specimens are shown in figure 33. The only unusual feature apparent on these specimens is that the initial crack propagation from the end of the fatigue crack was inclined 45° to 60° with respect to the tensile axis for specimens CNL-1U and CNL-1O. By contrast, initial crack propagation on specimen CNL-1P was essentially normal to the tensile axis as would be expected. The growth of the crack out of the normal fracture plane will tend to result in higher calculated toughness values. No metallurgical reason for growth out of the plane was apparent.

Conclusions: The high-toughness values were apparently due to crack deviation from the plane normal to the tensile axis.

Specimens CNL-1P and CNL-5P.—A significant difference in fatigue-crack-propagation rates was observed as a function of specimen thickness for the 36-inch-wide panels when tested under the same test conditions. Crack growth rates as functions of stress intensity factors extracted from the reported data are summarized in table VII.

TABLE VII
SUMMARY OF FATIGUE CRACK GROWTH DATA

Spec. no.	$K = 15 \text{ ksi}\sqrt{\text{in.}}$	$K = 25 \text{ ksi}\sqrt{\text{in.}}$	$K = 40 \text{ ksi}\sqrt{\text{in.}}$
CNL-1P 0.16 plate thickness	$da/dN = 10 \mu\text{in.}/N$	$da/dN = 50 \mu\text{in.}/N$	$da/dN = 350 \mu\text{in.}/N$
CNL-5P 0.50 plate thickness	$da/dN = 50 \mu\text{in.}/N$	$da/dN = 200 \mu\text{in.}/N$	$da/dN = 600 \mu\text{in.}/N$

Results: Profiles of the fractures are shown in figure 33. An examination of the fracture surface at six crack lengths verified the marked difference in crack propagation rates as indicated by the striation spacing. Typical fractographic examples showing the relative spacing are presented in figure 34. No metallurgical variation that could account for the effect was observed.

In thicker material (essentially plane strain), the average size of the plastic zone in front of a crack is smaller than for thin material (essentially plane stress) at the same K level. It has been proposed that the mechanical fatigue damage accumulating over smaller average volumes will produce cracking at higher rates. However, no explanation for the limitation of this effect to the wide panels is apparent.

Conclusions: The fatigue-crack-growth rates on a microscale reflect the macroscopic observations. No metallurgical variables account for this variation. A possible explanation for this effect involves the ratio of plane-strain-to-plane-stress conditions across the crack front.

Specimens 2UL6, 2PL6, and 2OL6.—The precracked-Charpy-toughness values did not follow the same trends established in the center-cracked-panel tests. In particular, the 0.25-inch underaged material showed a higher than expected value as compared to the overaged material. The reported values are summarized in table VIII.

TABLE VIII
SUMMARY OF CHARPY TOUGHNESS DATA

Spec. no.	Grain direction	Heat treatment	$W/A, \text{in.-lb/in.}^2$
2UL6	Longitudinal	Underaged	535
2PL6	Longitudinal	Peak (T6)	347
2OL6	Longitudinal	Overaged	312

Results: The fractures are shown in figure 35. Sections through the fracture faces are shown in figures 36 and 37. No metallurgical or mechanical reasons for this difference in behavior were observed.

Conclusions: The reasons for this behavior were not determined.

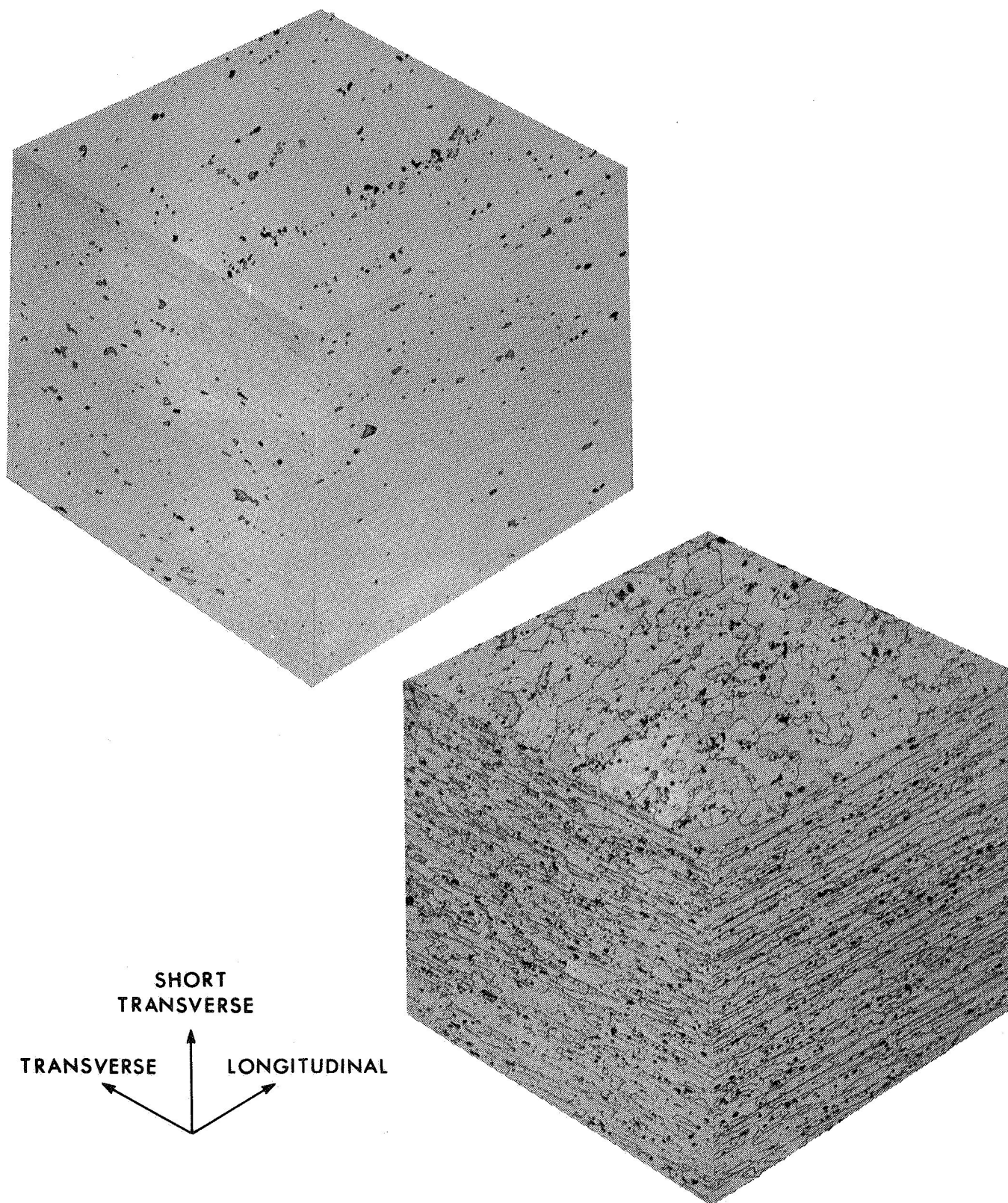


Figure 1. Light and normally etched microstructures of 0.160-inch-thick material in the underaged condition (Magnification 86.5X)

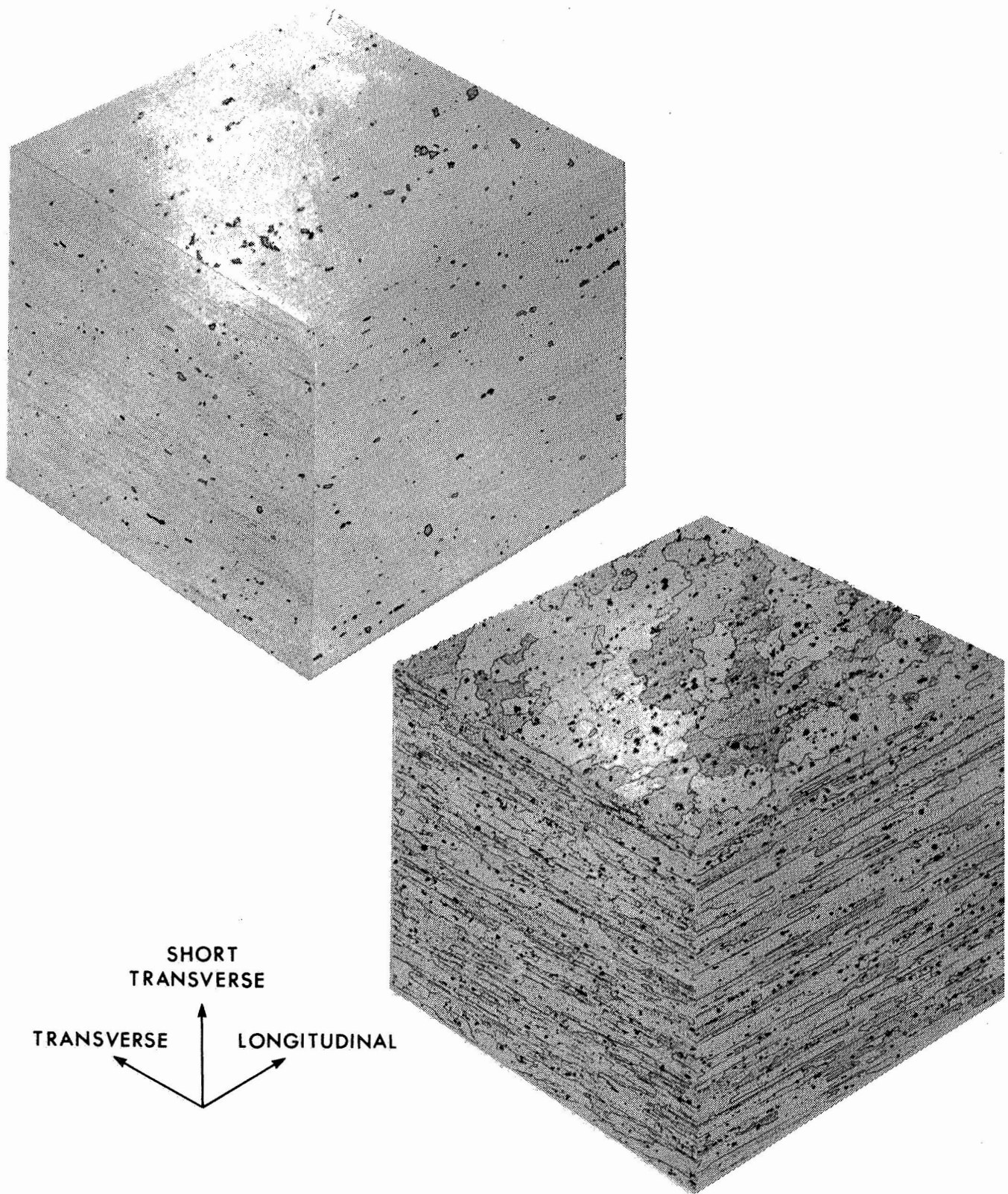


Figure 2. Light and normally etched microstructures of 0.250-inch-thick material in the underaged condition (Magnification 86.5X)

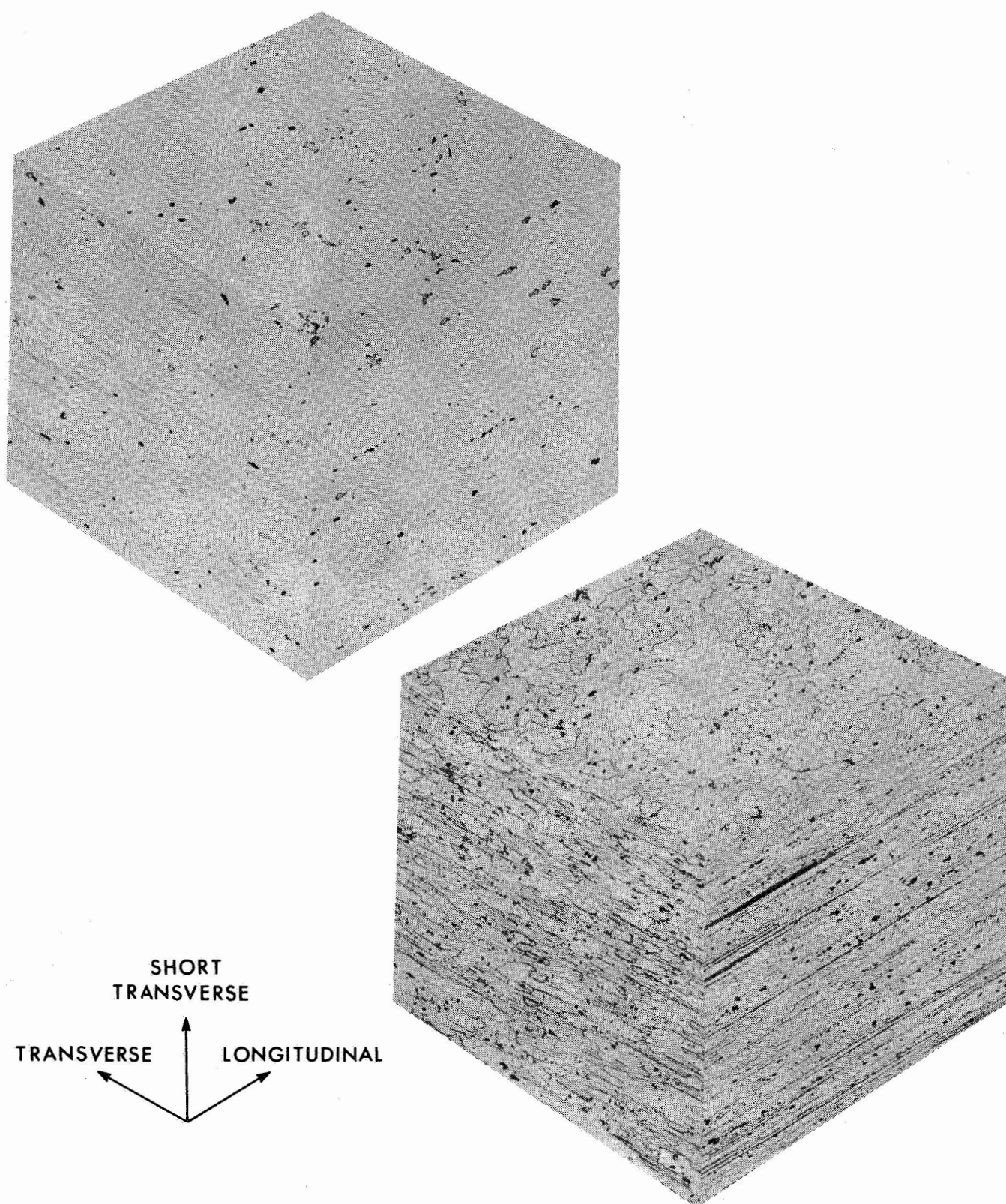


Figure 3. Light and normally etched microstructures of 0.500-inch-thick material in the underaged condition (Magnification 86.5X)

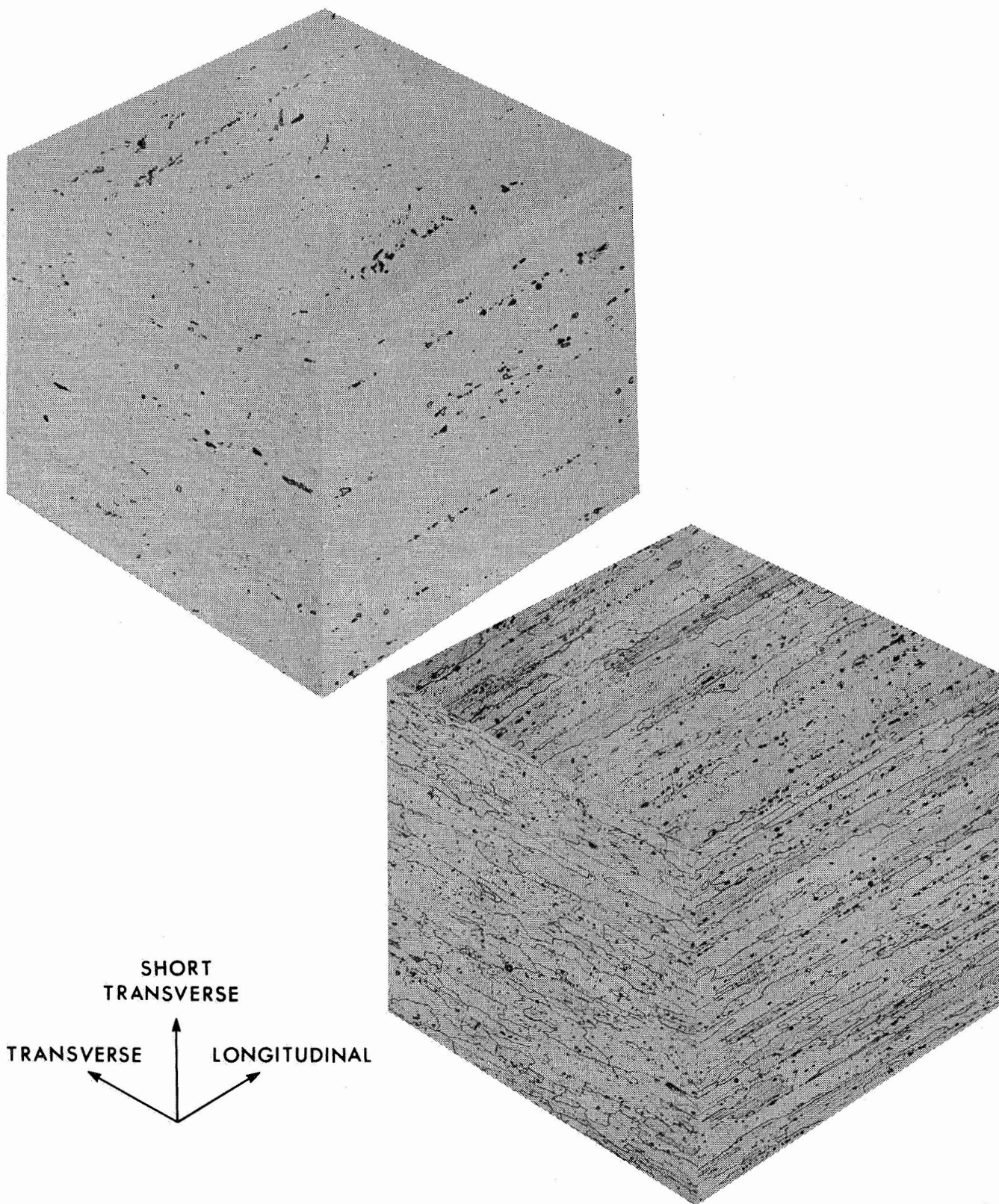


Figure 4. Light and normally etched microstructures of 0.630-inch-thick material in the underaged condition near the plate edge (Magnification 86.5X)

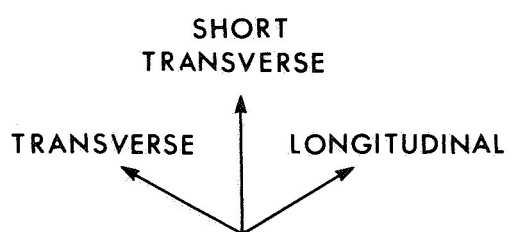
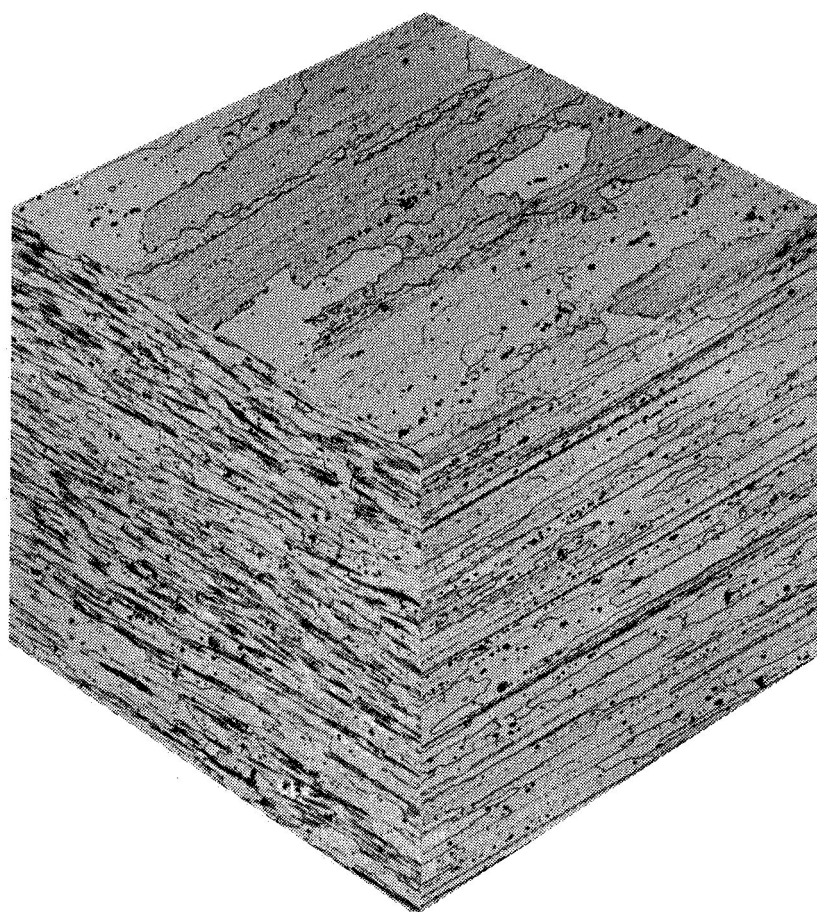


Figure 5. Light and normally etched microstructures of 0.630-inch-thick material in the underaged condition near the plate center (Magnification 86.5X)

VARIATIONS OF MICROSTRUCTURE THROUGH ROLLED PLATES OF 7079
UNDERAGED.

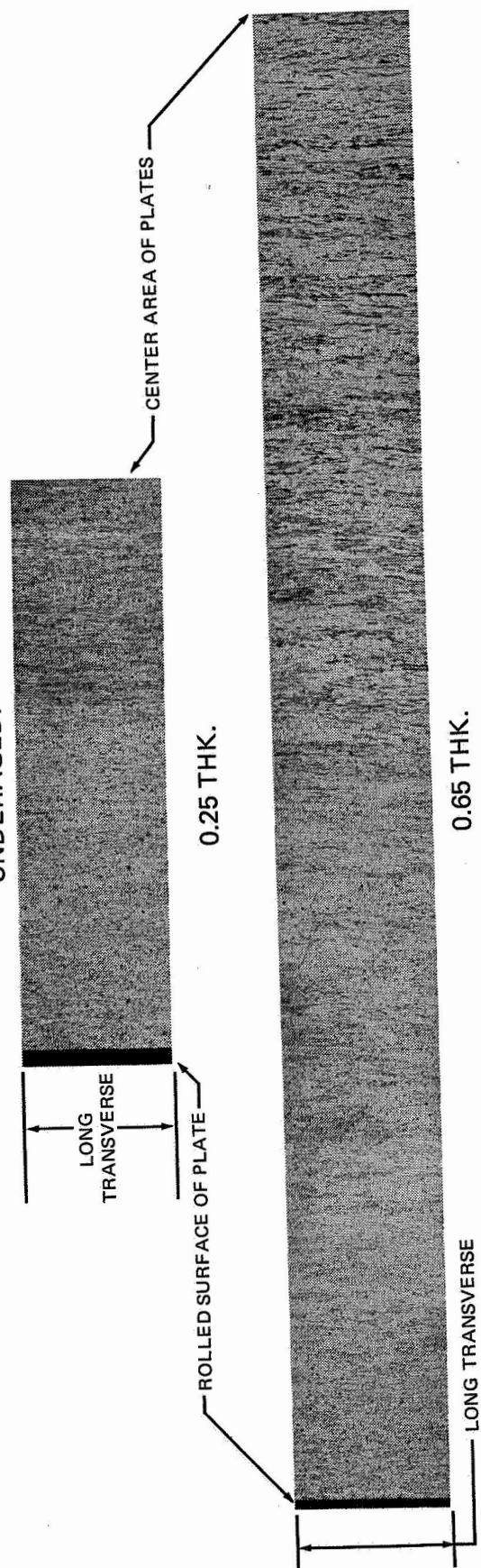


Figure 6. Microstructure as a function of thickness in 0.250 and 0.630-inch-thick material
(Magnification 27X)

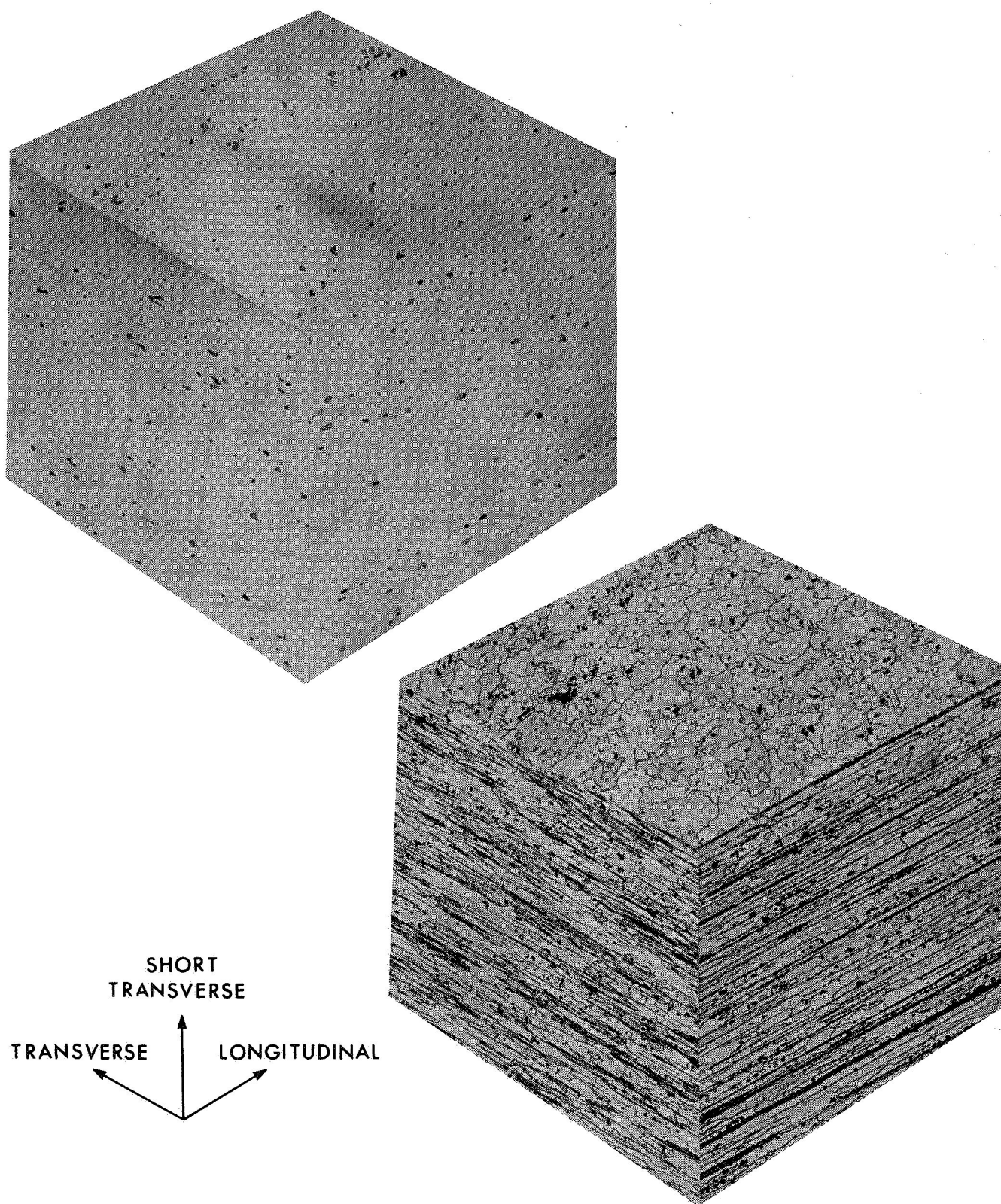


Figure 7. Light and normally etched microstructures of 0.250-inch-thick material in the peak-aged (T6) condition (Magnification 86.5X)

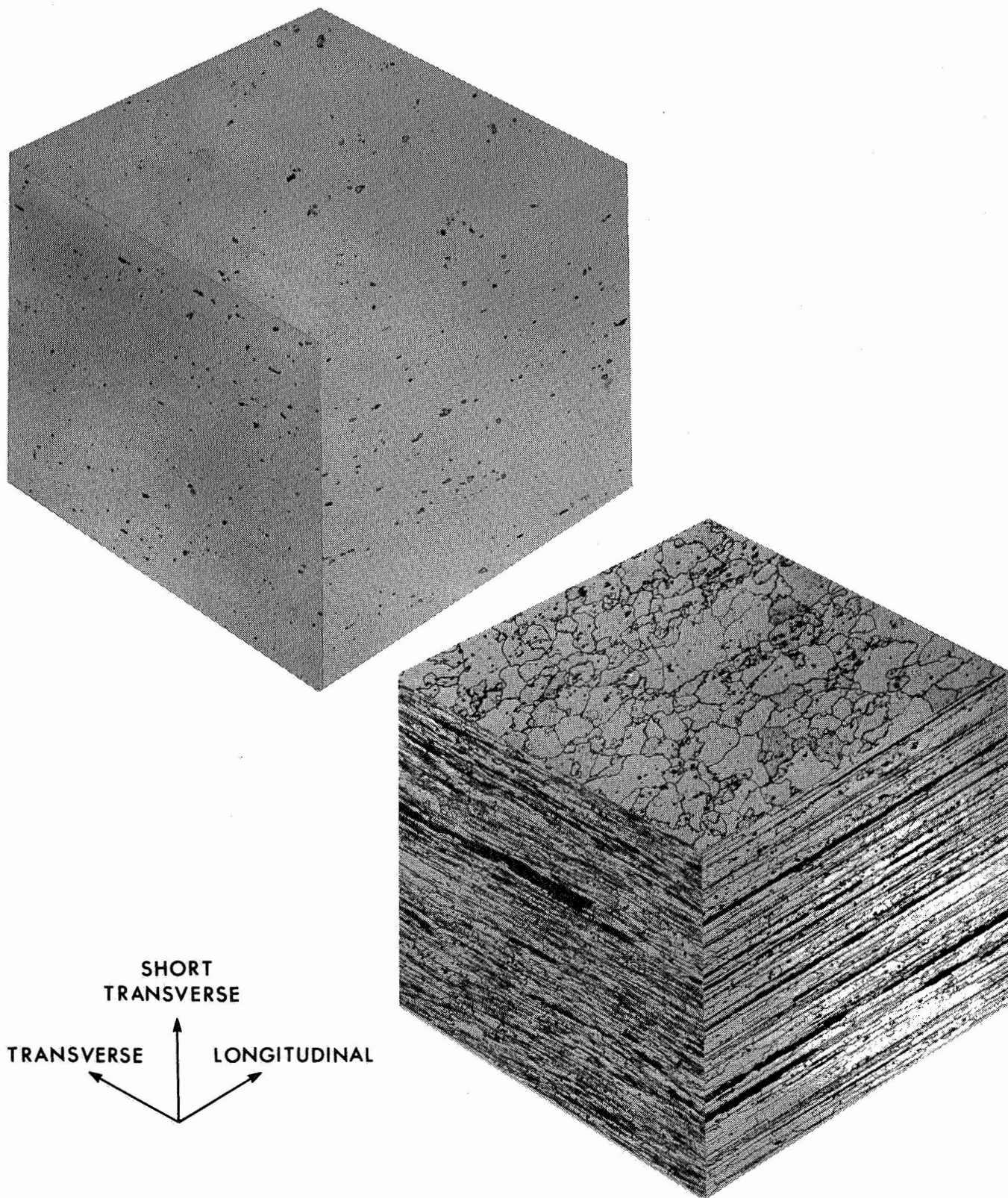


Figure 8. Light and normally etched microstructures of 0.250-inch-thick material in the overaged condition (Magnification 86.5X)

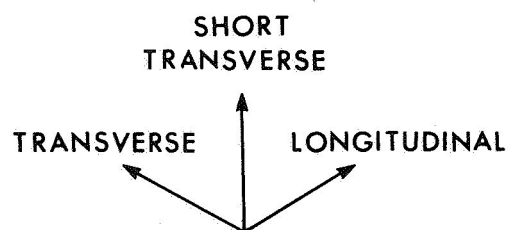
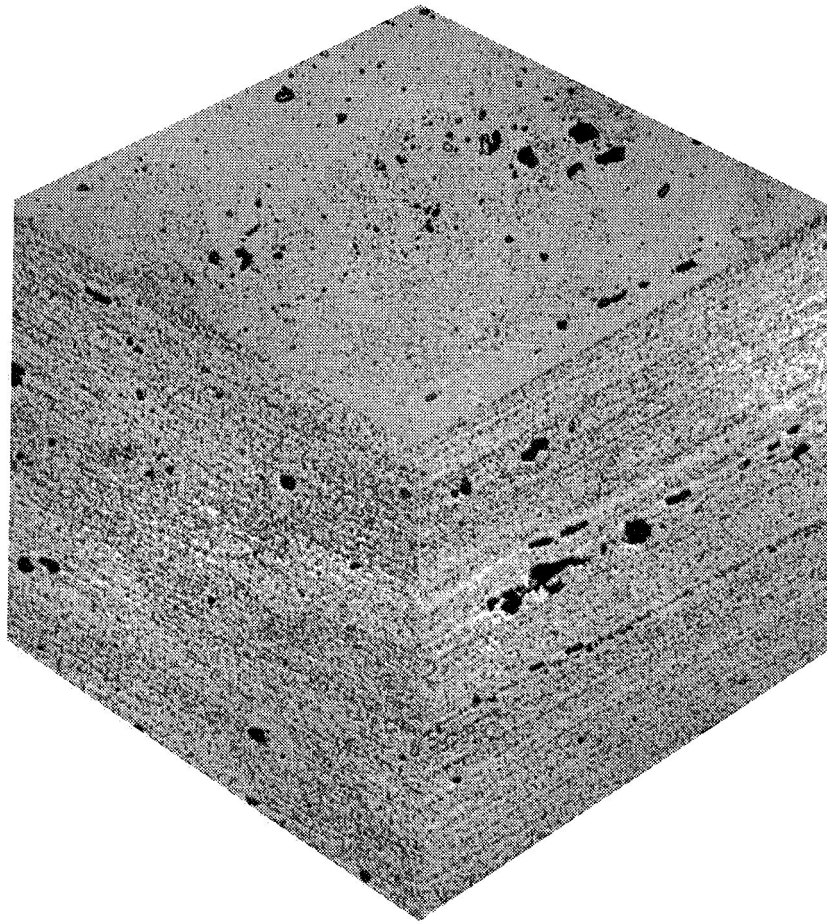


Figure 9. Microstructure of 0.25-inch-thick material in the underaged condition (Magnification 440X)

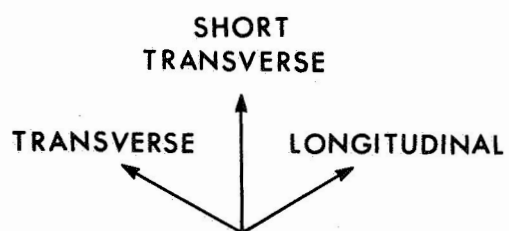
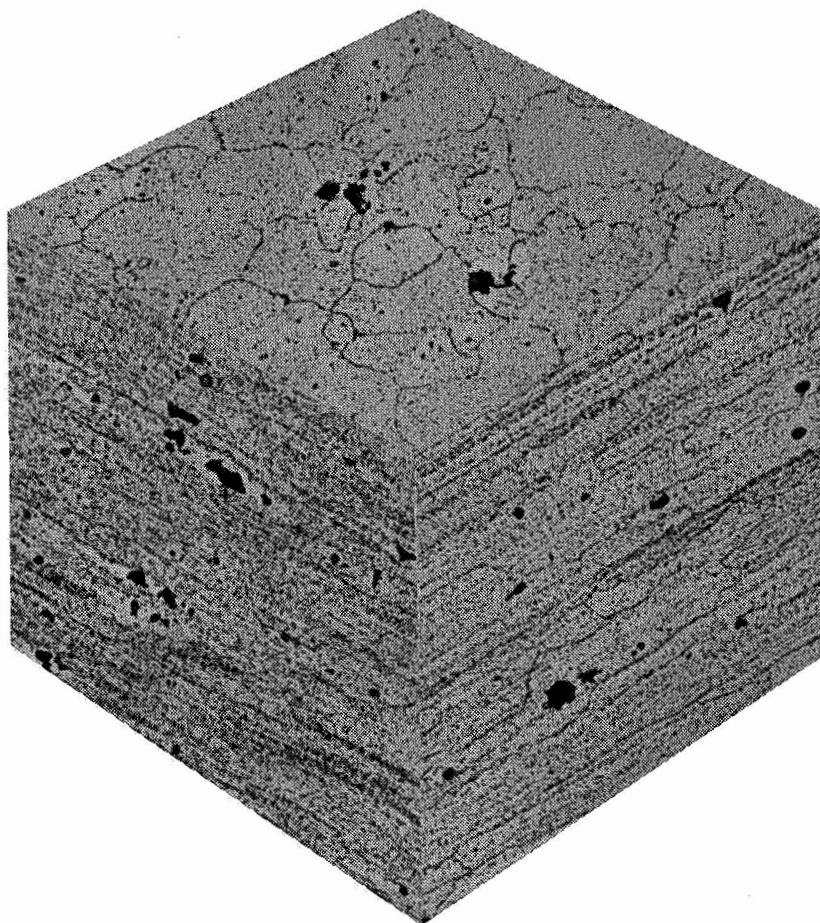


Figure 10. Microstructure of 0.25-inch-thick material in the peak-aged (T6) condition (Magnification 440X)

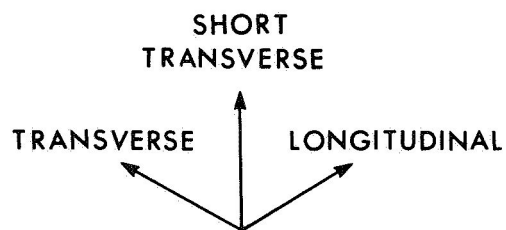
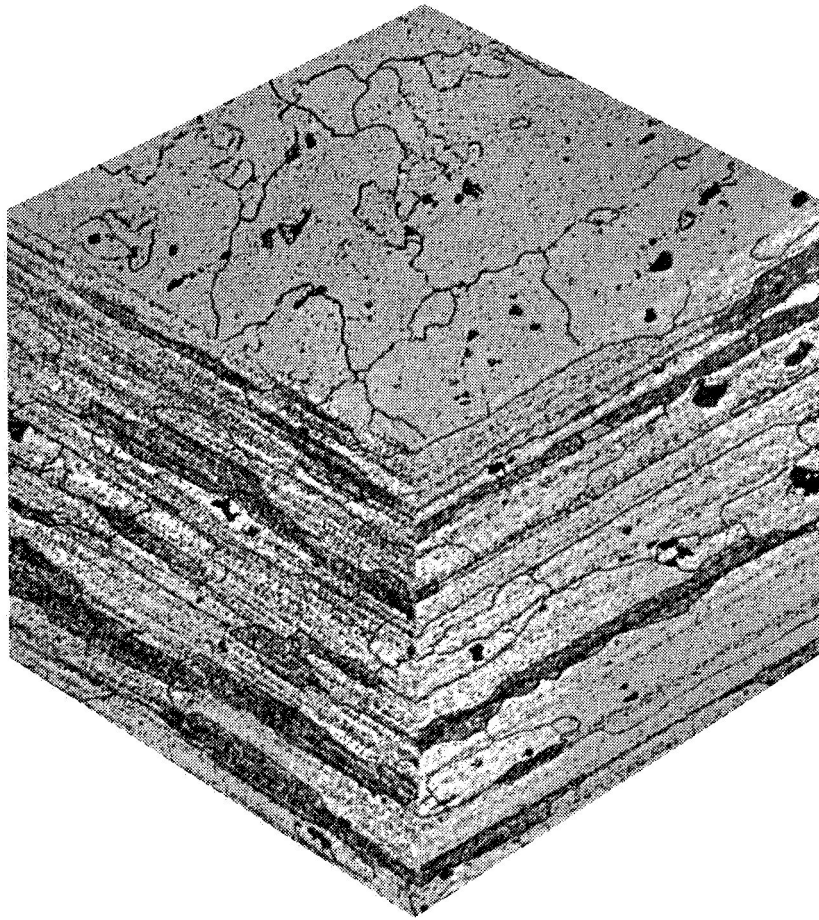
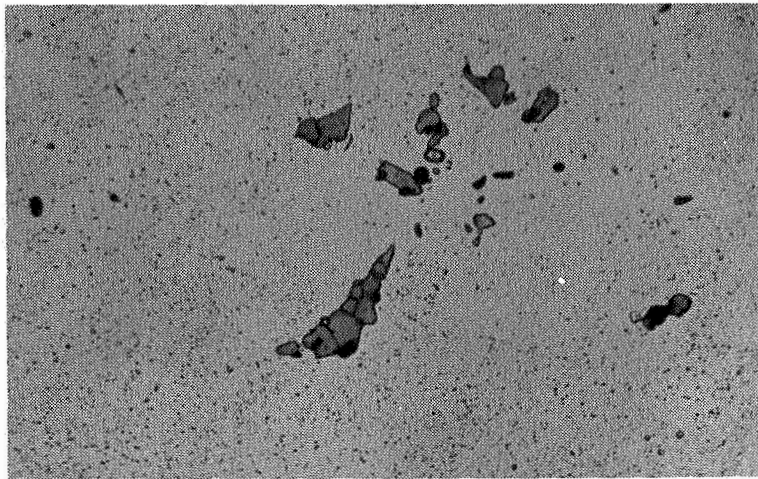
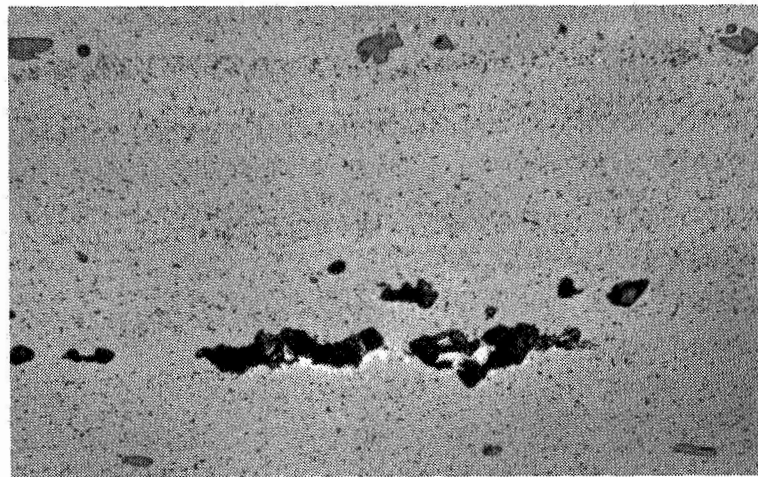


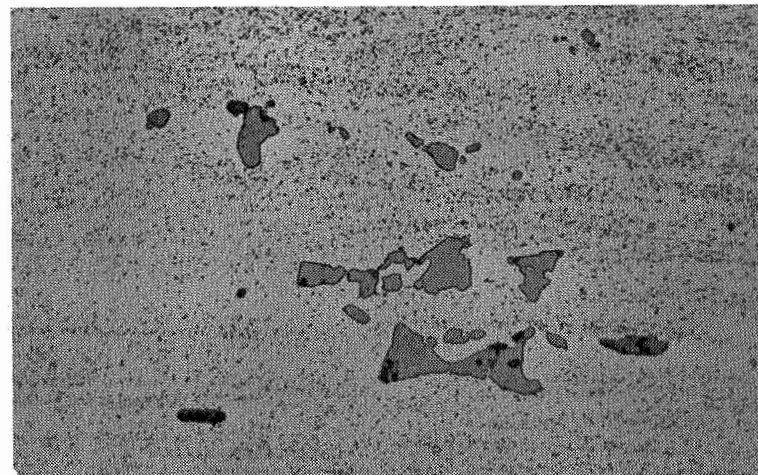
Figure 11. Microstructure of 0.25-inch-thick material in the overaged condition (Magnification 440X)



(a) Short transverse view

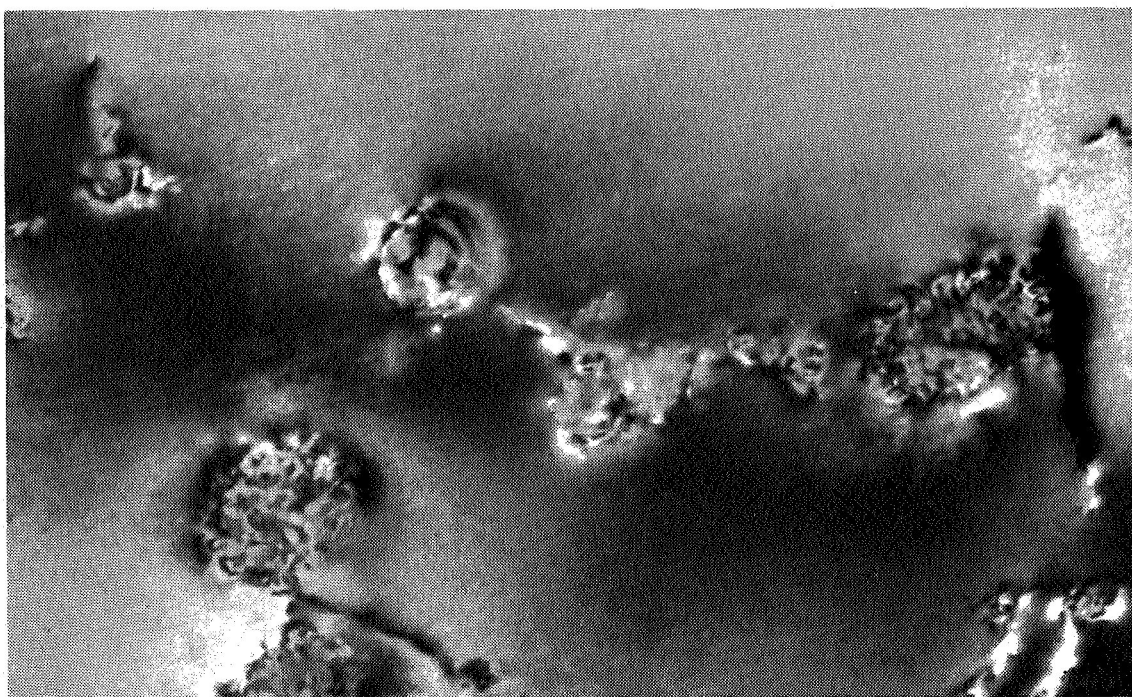


(b) Long transverse view

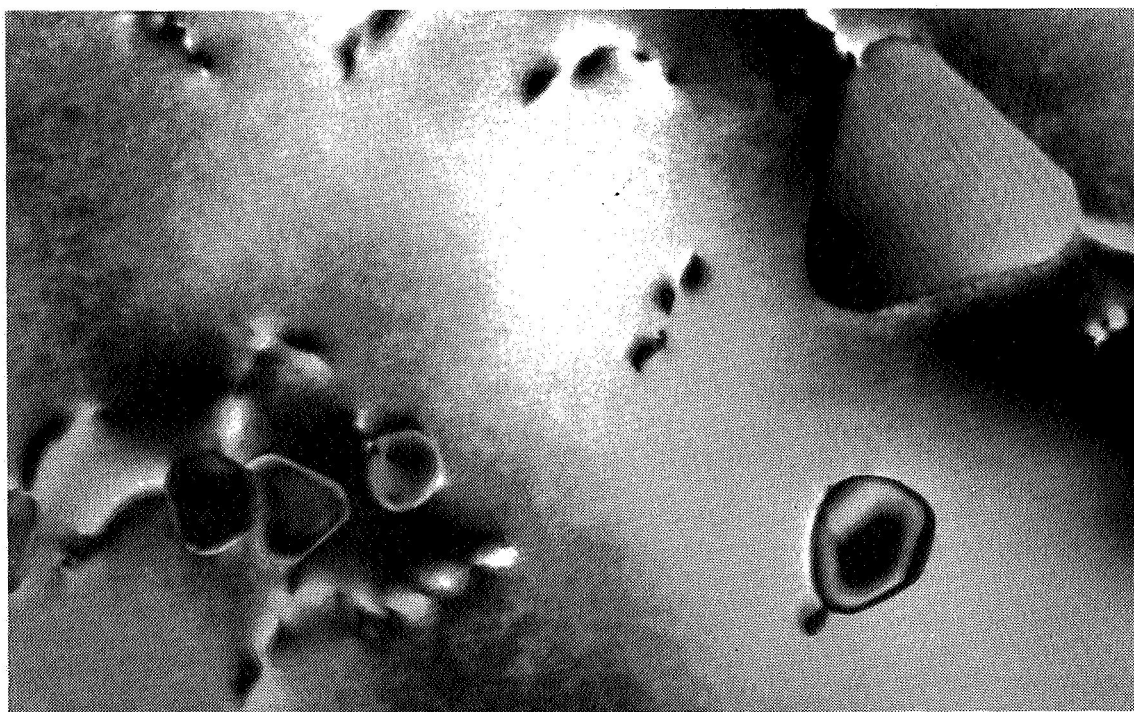


(c) Longitudinal view

Figure 12. Large intermetallics observed in the 0.500-inch-thick underaged material (Magnification 1000X)

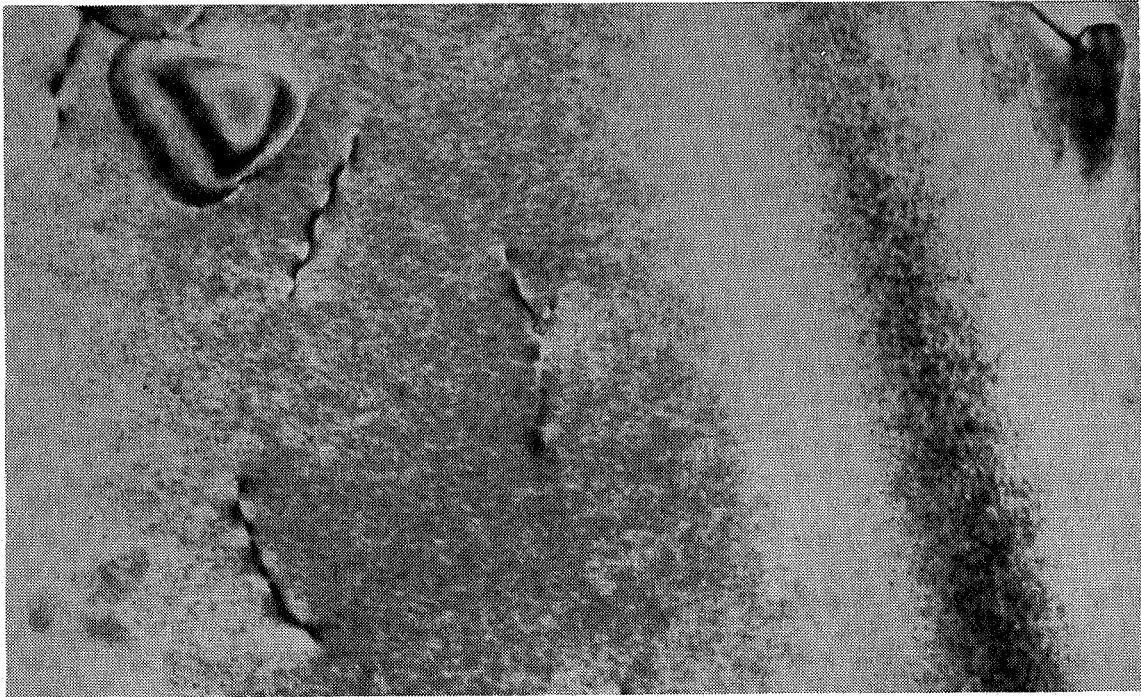


(a) Solution-treated material [100] zone normal

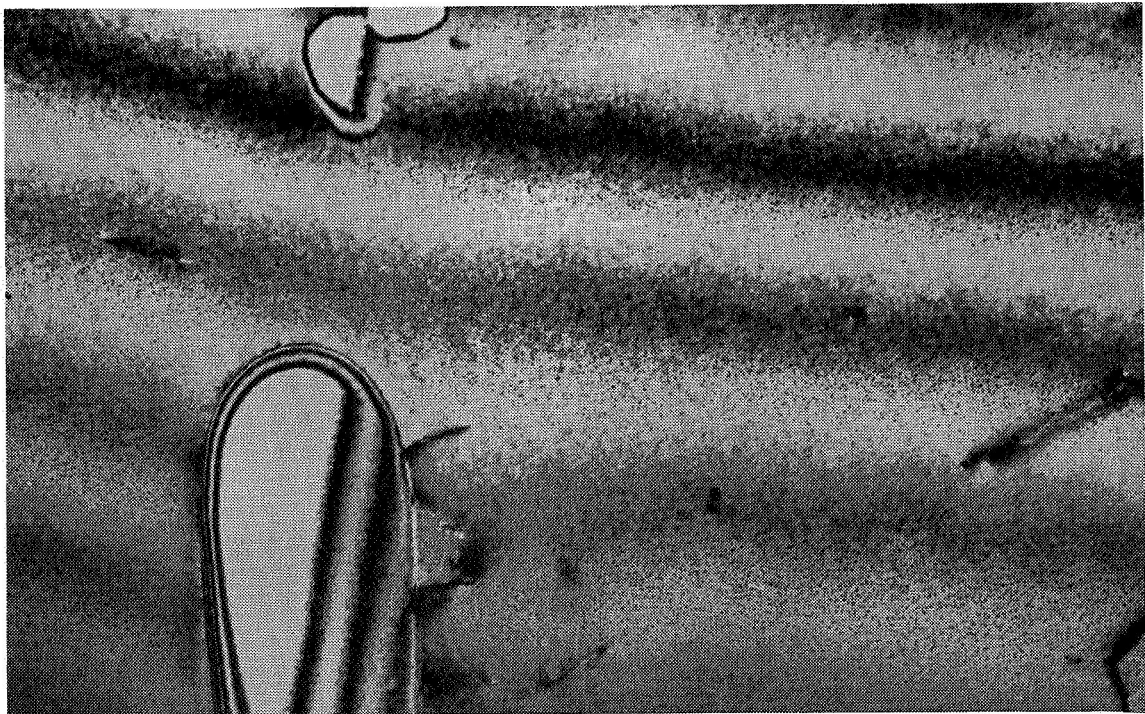


(b) Solution-treated plus a 10-day room-temperature age [100] zone normal

Figure 13. *Transmission electron micrographs (no hardening precipitate can be seen in the structure) (Magnification 150 000X)*

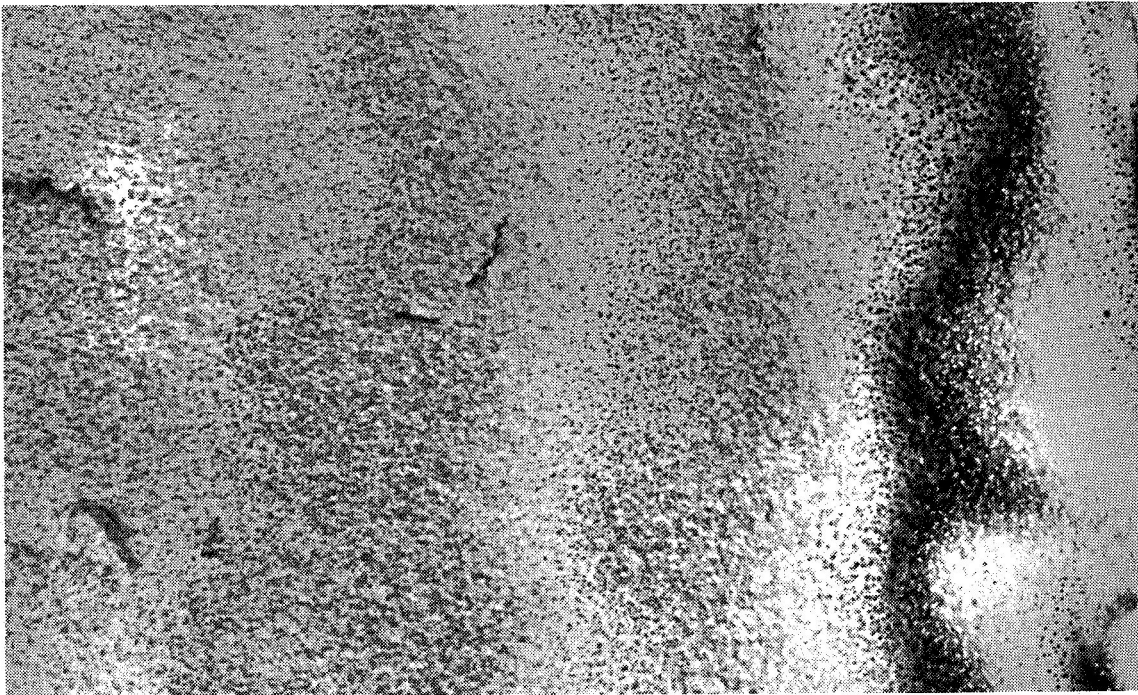


(a) Material aged 10 minutes at 250° F, [110] zone normal (Magnification 150 000X)

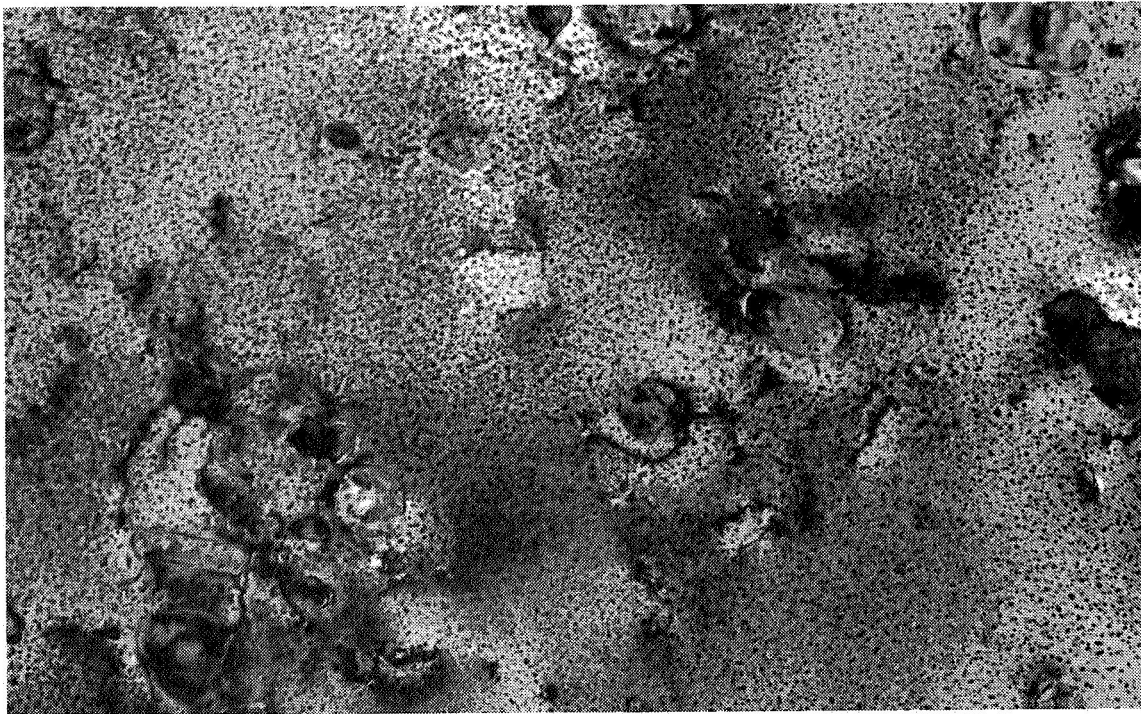


(b) Material aged 2 hours at 250° F [110] zone normal (Magnification 84 000X)

Figure 14. *Transmission electron micrographs (the hardening precipitate can be observed as a very fine scale dispersion of particles in the matrix)*

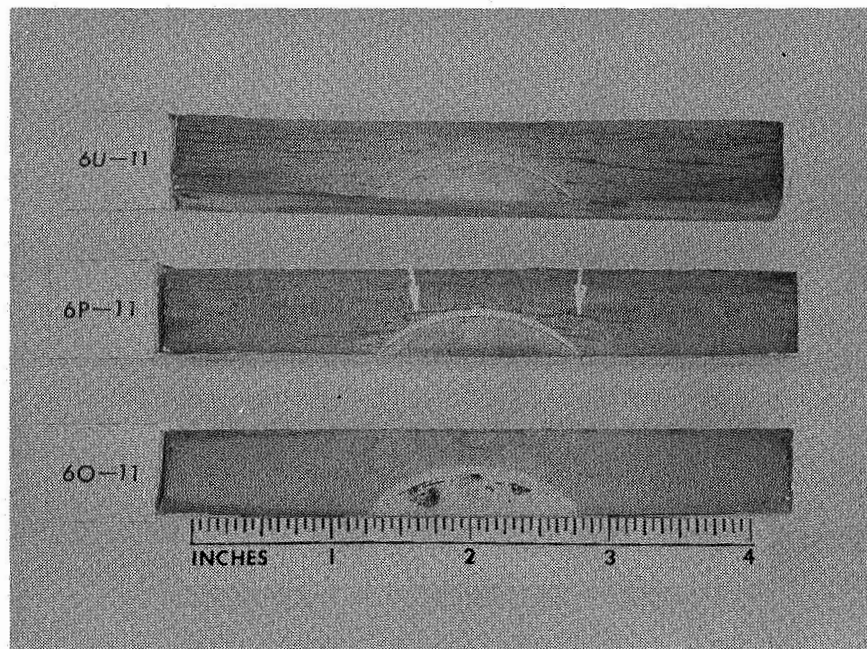


(a) Material aged 30 hours at 250° F, [110] zone normal (Magnification 115 000X)



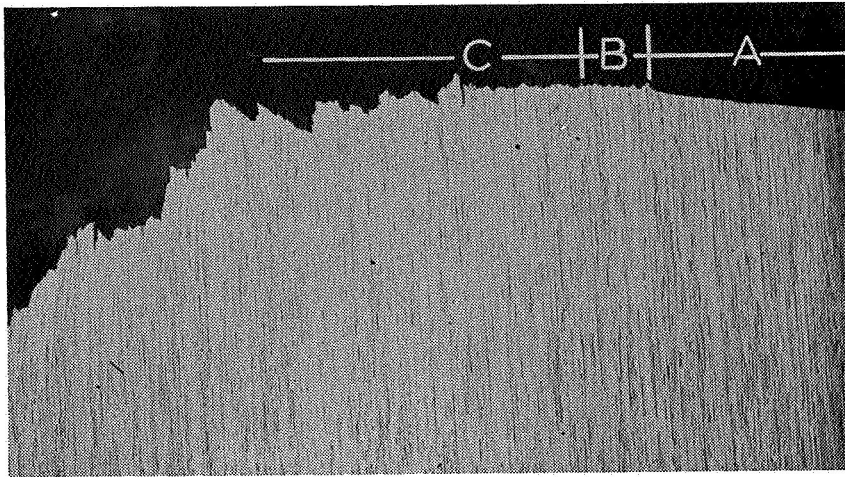
(b) Material aged 60 hours at 290° F, [110] zone normal (Magnification 69 000X)

Figure 15. *Transmission electron micrographs (the hardening precipitate can be observed as a very fine scale dispersion of particles in the matrix)*

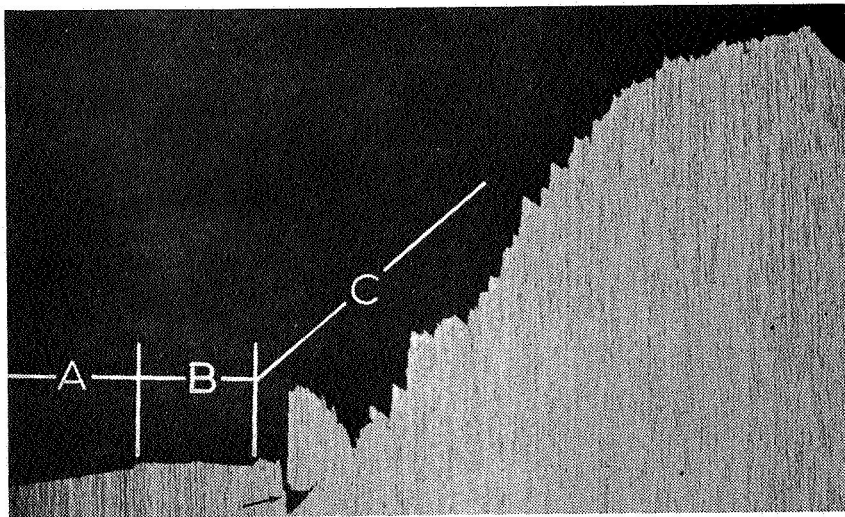


NOTE: Arrows indicate a transverse split or delamination in specimen 6P-11

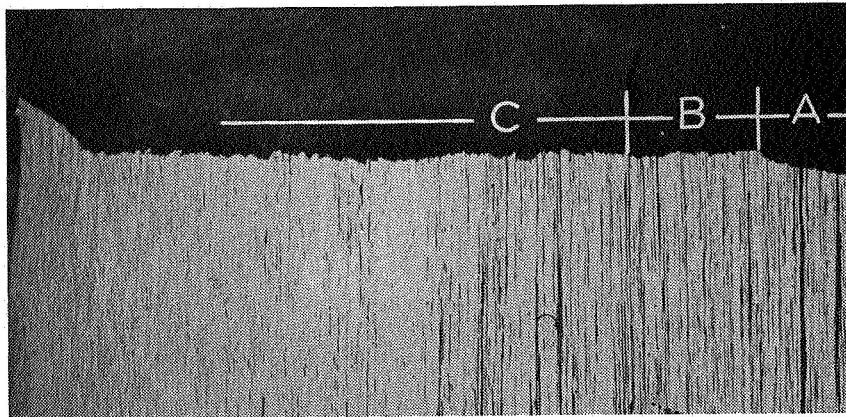
Figure 16. Macroscopic view of surface-flawed fracture-toughness specimens



Underaged heat-treatment condition



Peak-aged (T6) heat-treatment condition



Overaged heat-treatment condition

NOTE: A indicates region of machined notch, B indicates region of fatigue pre crack, C indicates region of fast fracture (Magnification 10X)

Figure 17. Fracture profiles of surface-flawed fracture-roughness specimens: underaged, peak aged (T6), and overaged heat treatment condition.

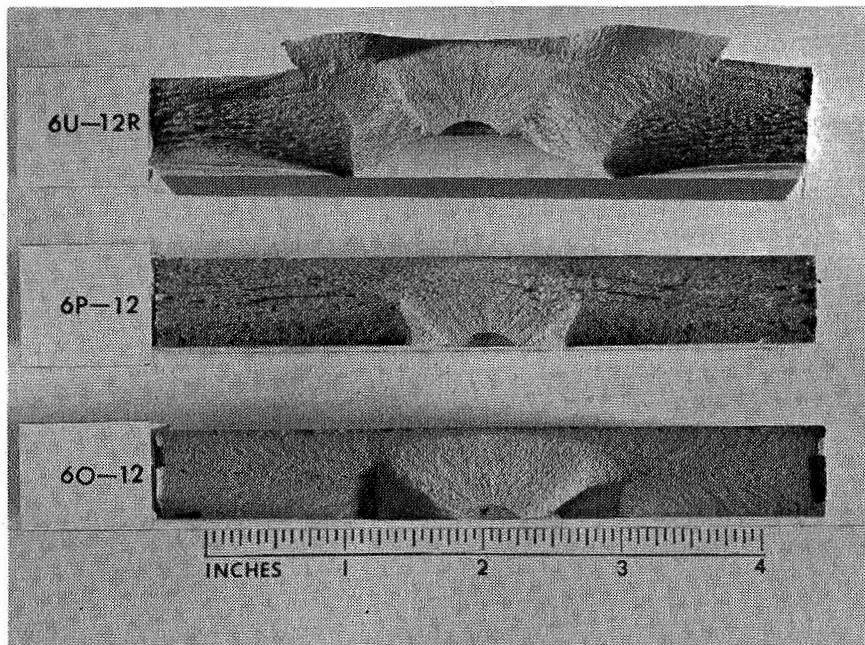


Figure 18. Macroscopic view of surface-flawed fatigue specimens

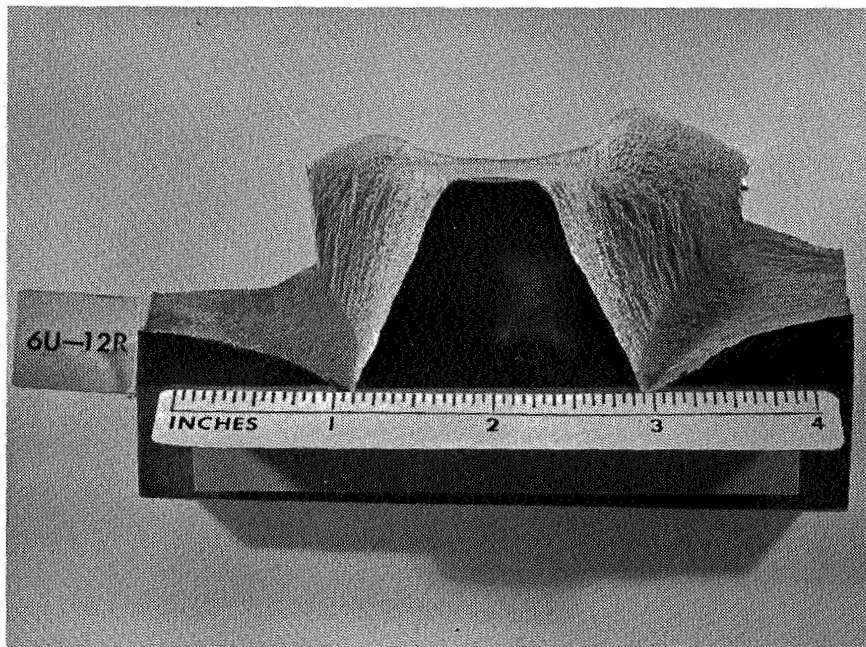
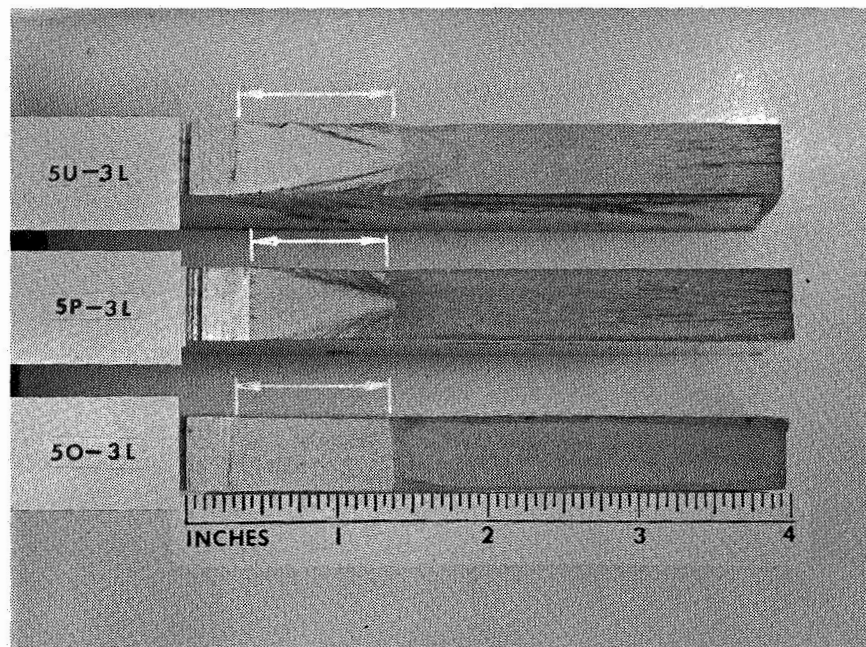
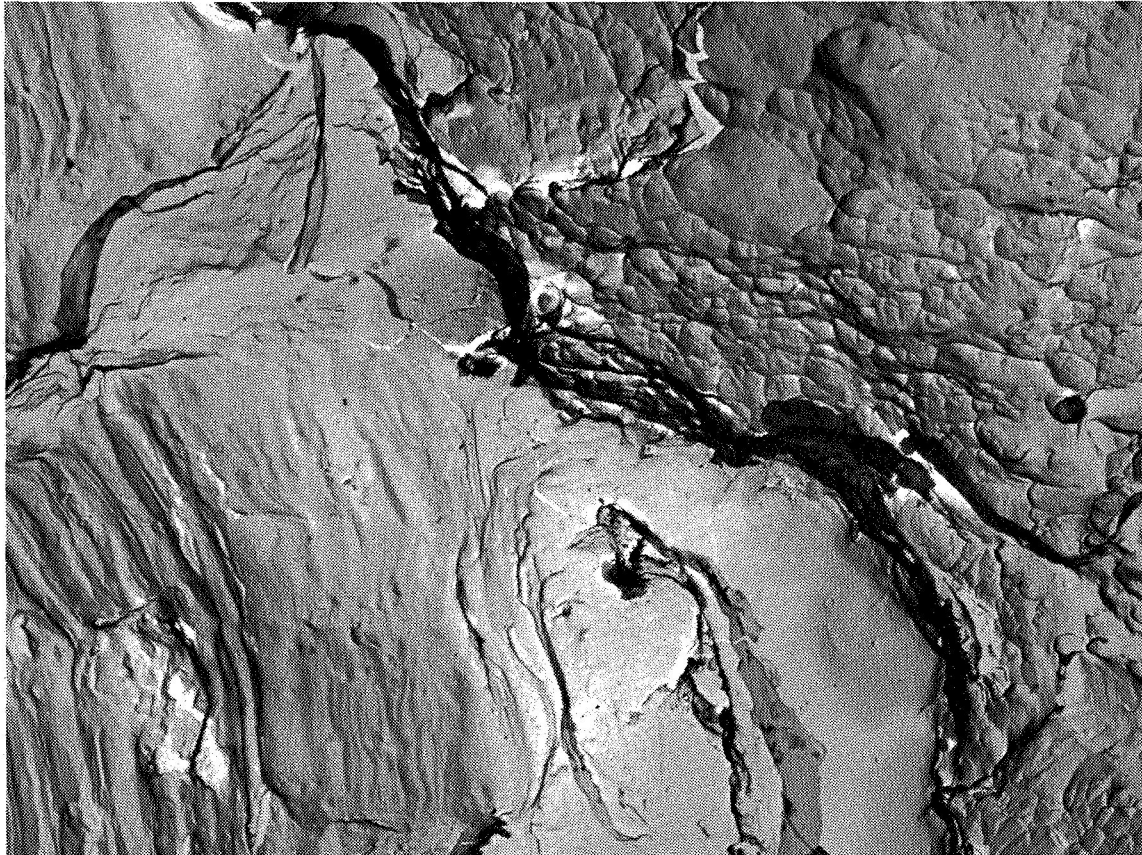


Figure 19. Unusual fracture appearance of underaged specimen



NOTE: Arrows indicate the extent of the fatigue zone

Figure 20. Macroscopic view of 0.500-inch-thick center-notched fatigue panels

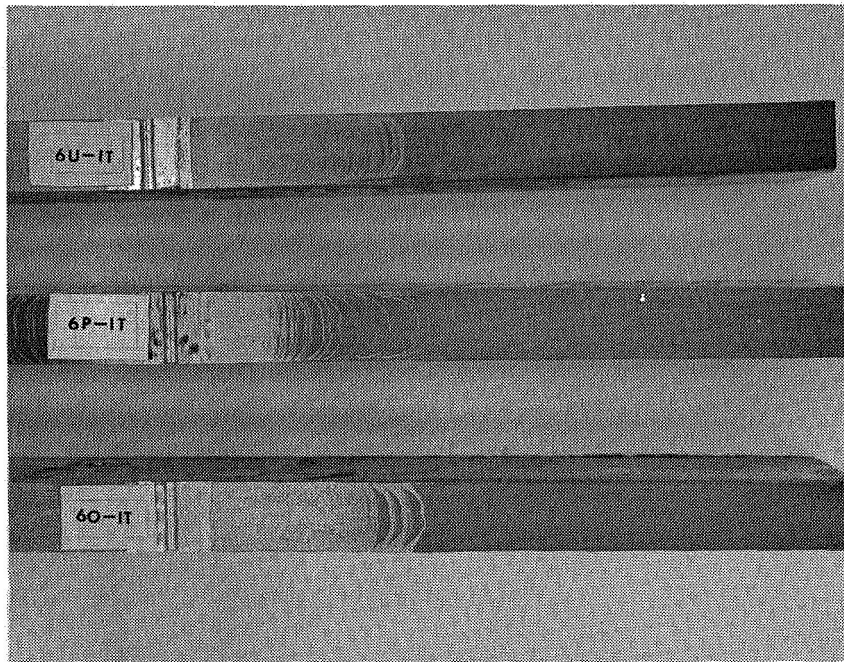


Fatigue

Stretched Zone

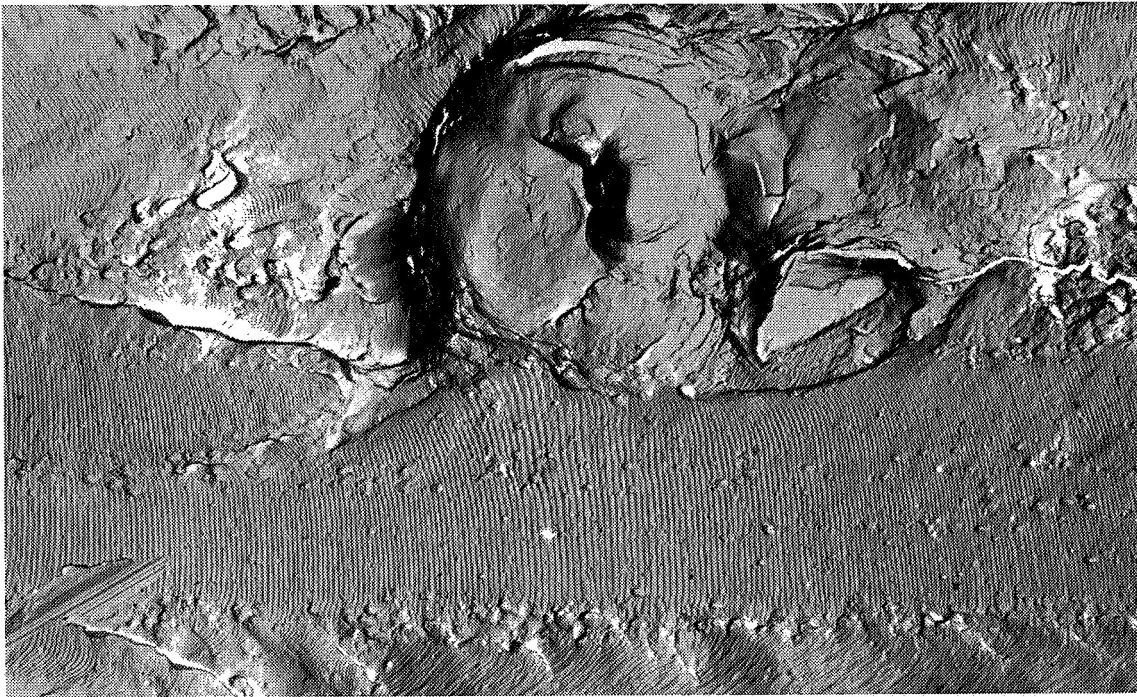
Fast fracture

Figure 21. Electron fractograph of the fatigue-to-fast-fracture interface for the underaged specimen (Magnification 3200X)



NOTE: Specimens designated -1T and -2T were tested in dry air and distilled water respectively (Magnification approximately 1/2X)

Figure 22. Macroscopic view of 0.63-inch-thick center-notched fatigue specimens

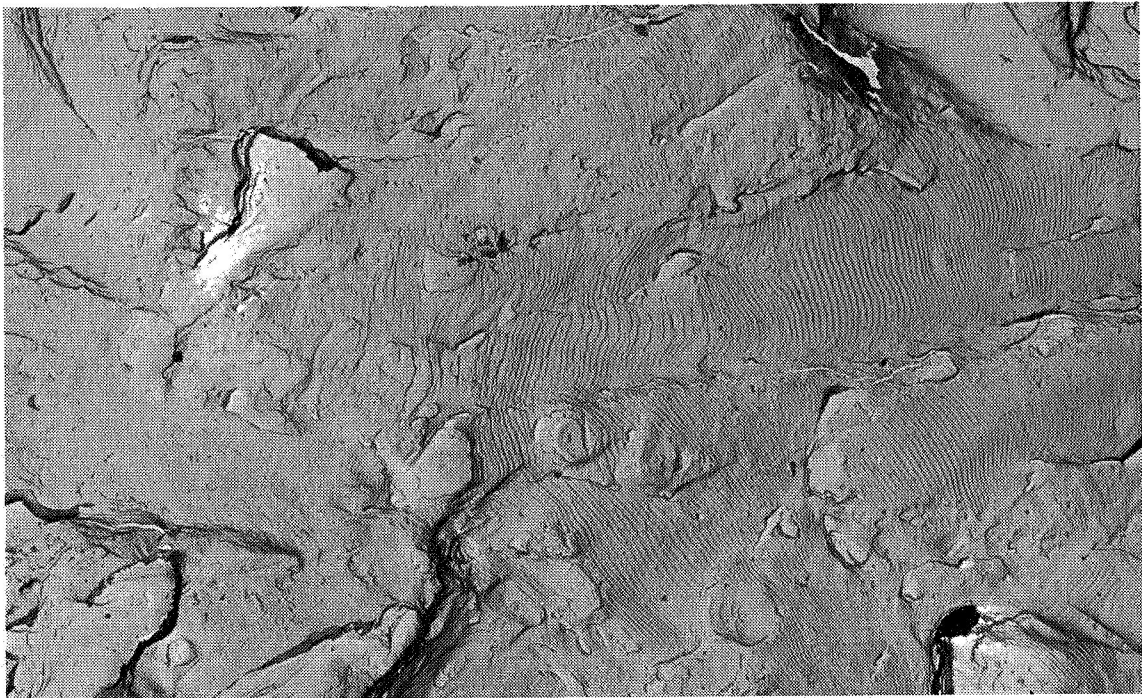


(a) Dry-air environment

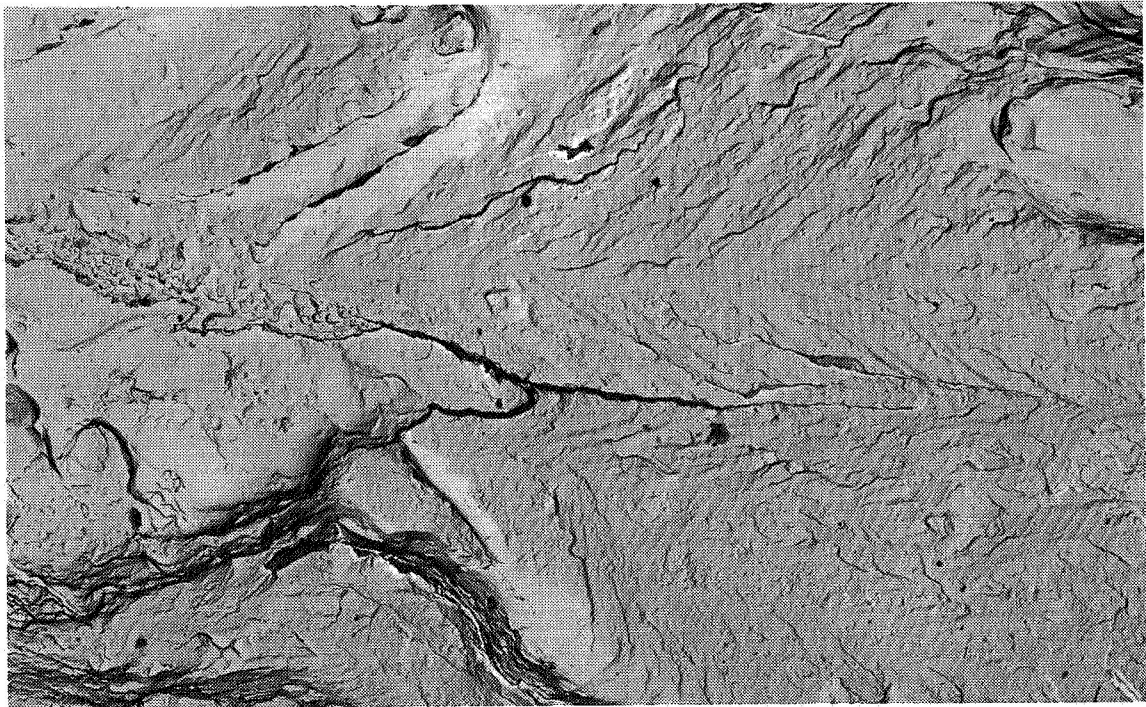


(b) Distilled-water environment

Figure 23. *Electron fractographic comparison of the fatigue-fracture mode for the 0.25-inch-thick underaged material at $2a = 2.00$ inches (Magnification 3200X)*

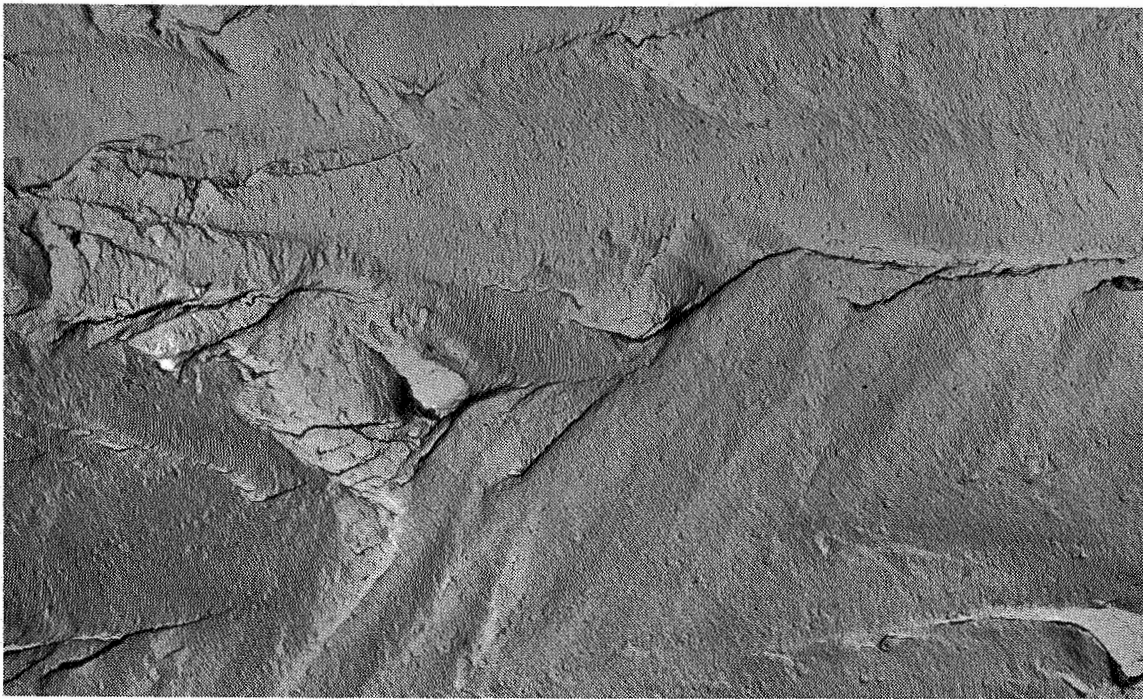


(a) Dry-air environment

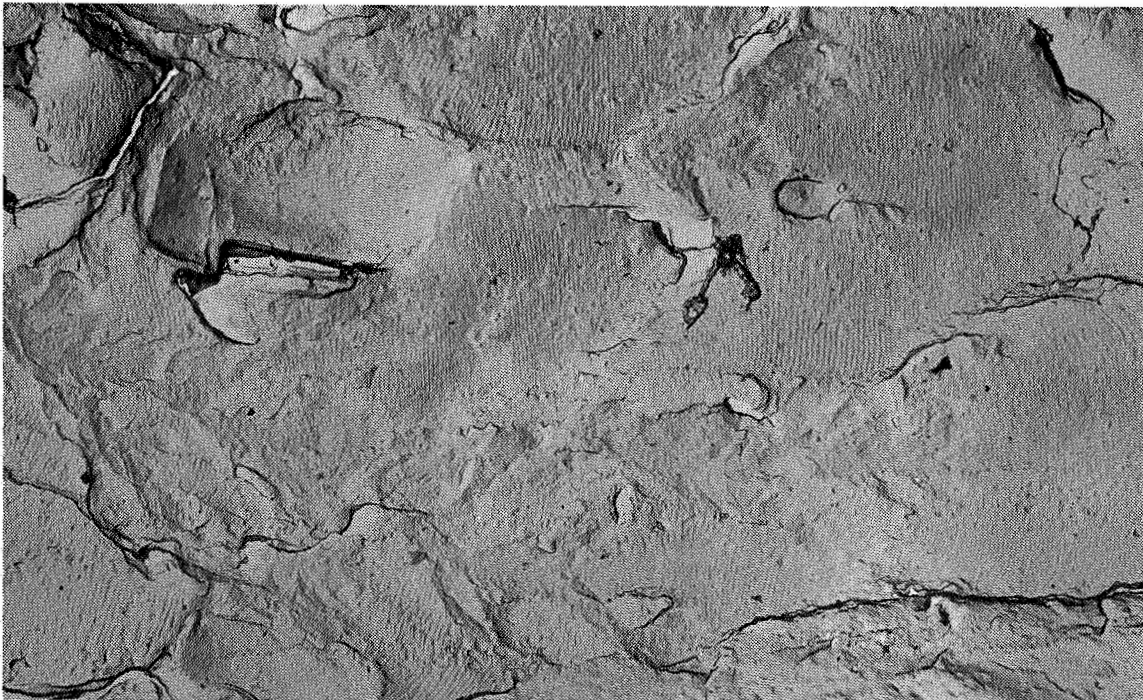


(b) Distilled-water environment

Figure 24. *Electron fractographic comparison of the fatigue-fracture mode for the 0.25-inch-thick peak-aged (T6) material at $2a = 2.00$ inches (Magnification 3200X)*



(a) Dry-air environment

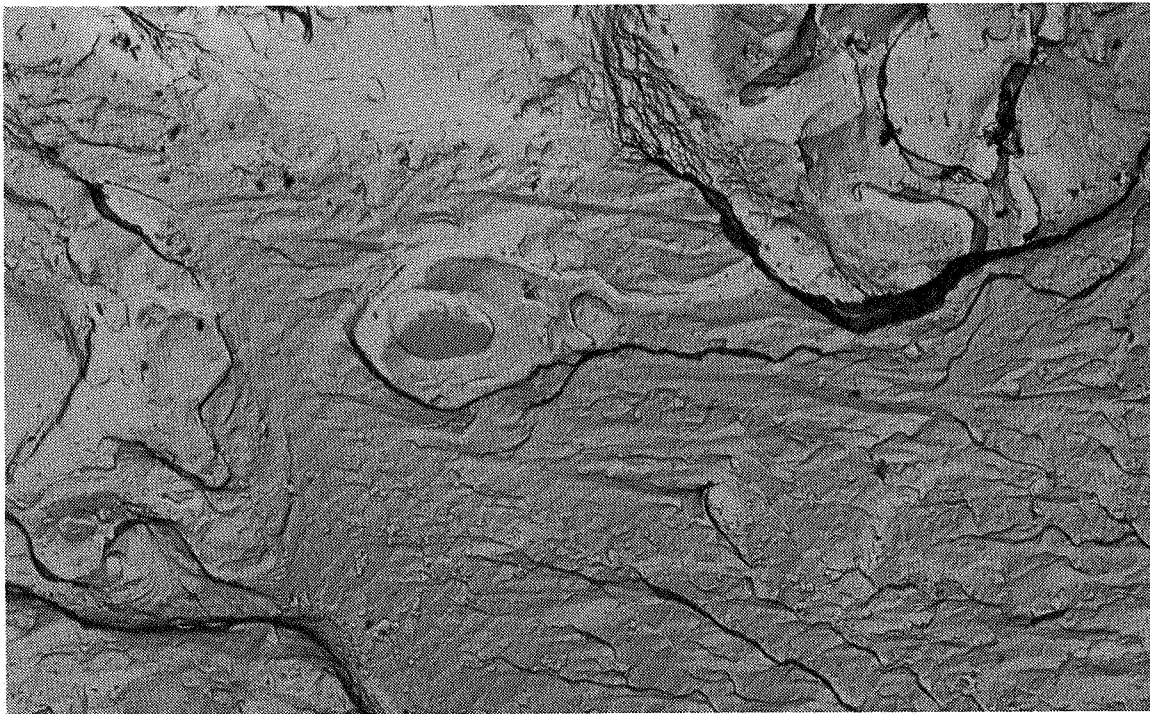


(b) Distilled-water environment

Figure 25. *Electron fractographic comparison of the fatigue-fracture mode for the 0.25-inch-thick overaged material at $2a = 2.00$ inches (Magnification 3200X)*

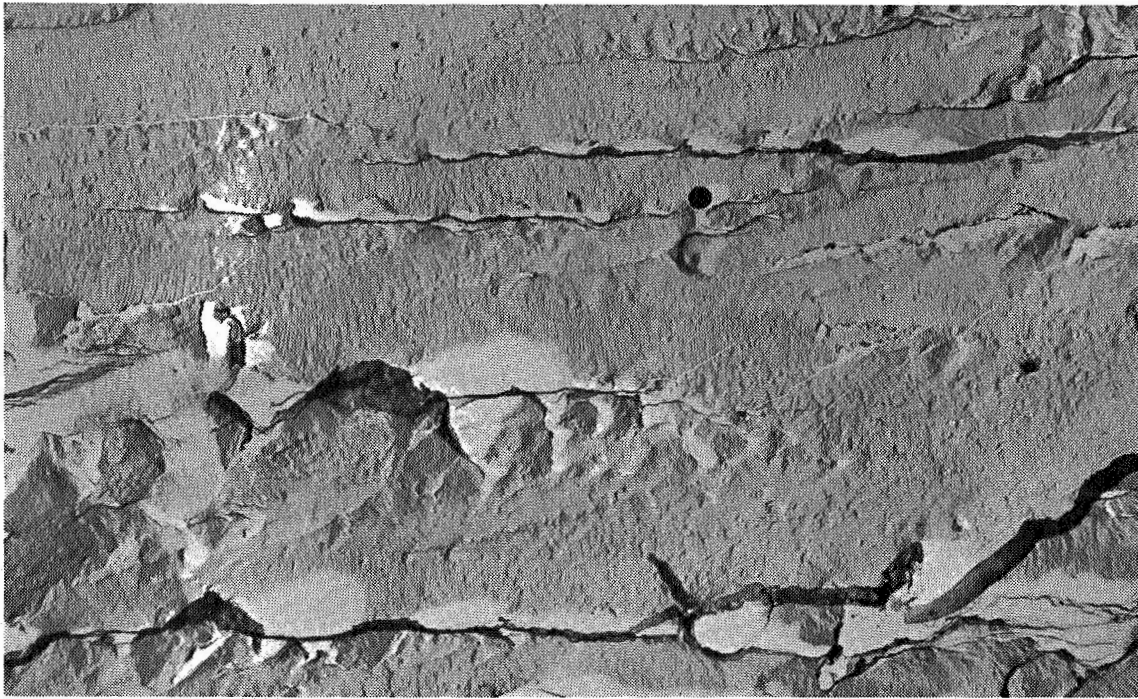


(a) Dry-air environment

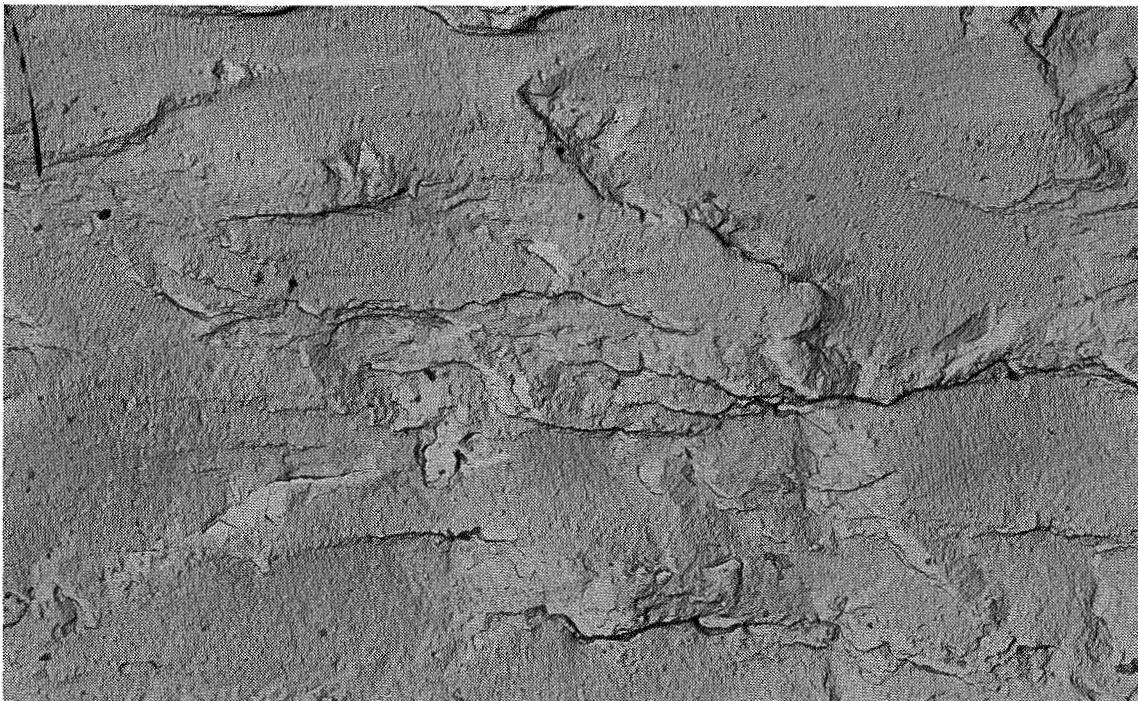


(b) Distilled-water environment

Figure 26. *Electron fractographic comparison of the fatigue-fracture mode for the 0.63-inch-thick peak-aged (T6) material at $2a = 1.5$ inches (Magnification 2850X)*

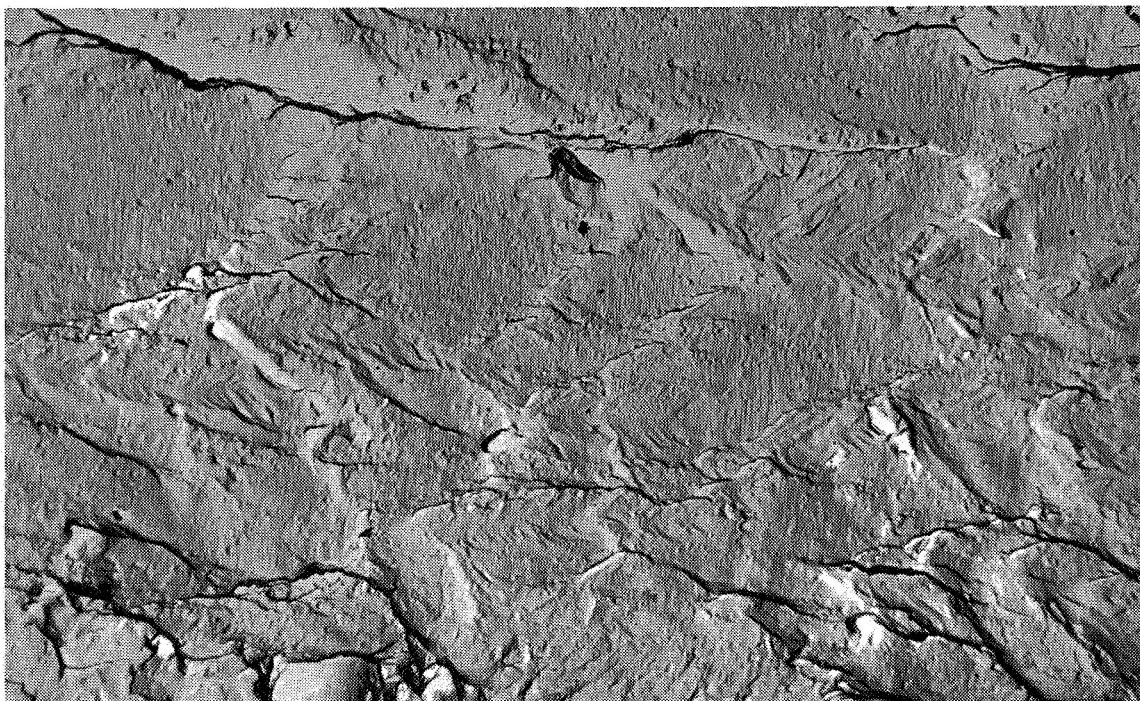


(a) Dry-air environment

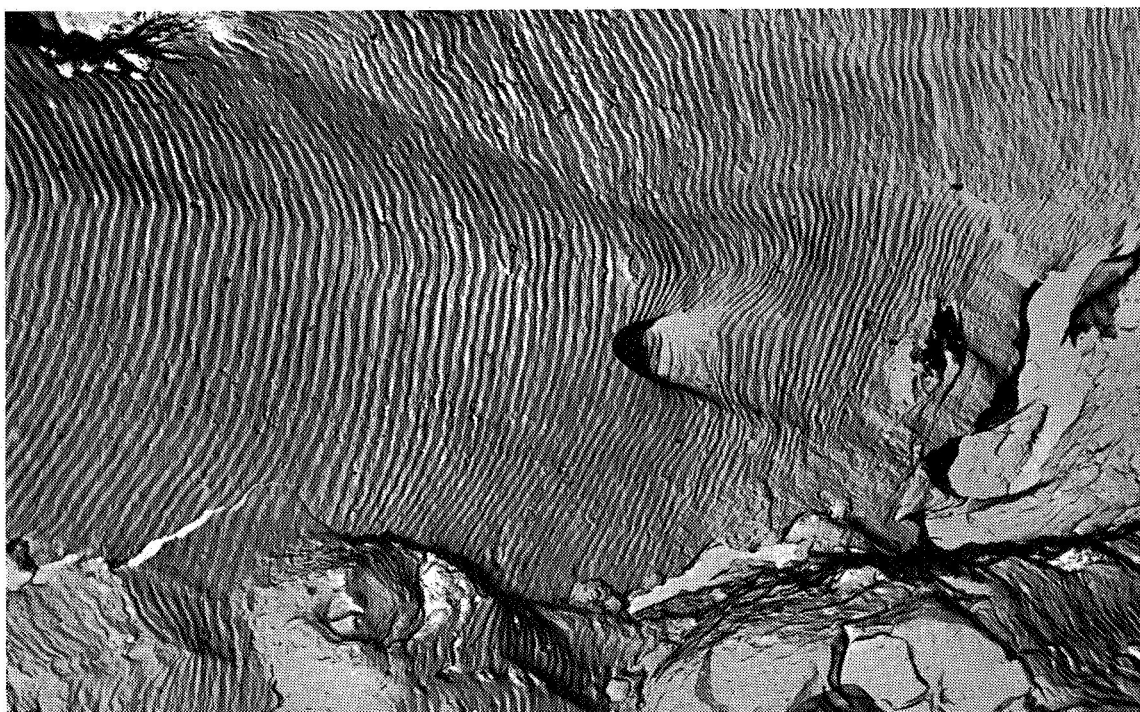


(b) Distilled-water environment

Figure 27. *Electron fractographic comparison of the fatigue-fracture mode for the 0.63-inch-thick overaged material at $2a = 1.5$ inches (Magnification 2850X)*



(a) $R = 0.67$



(b) $R = 0.05$

Figure 28. Electron fractographic comparison of 0.25-inch-thick underaged material tested at two stress ratios in a dry-air environment, $2a = 1.2$ inches (Magnification 3200X)

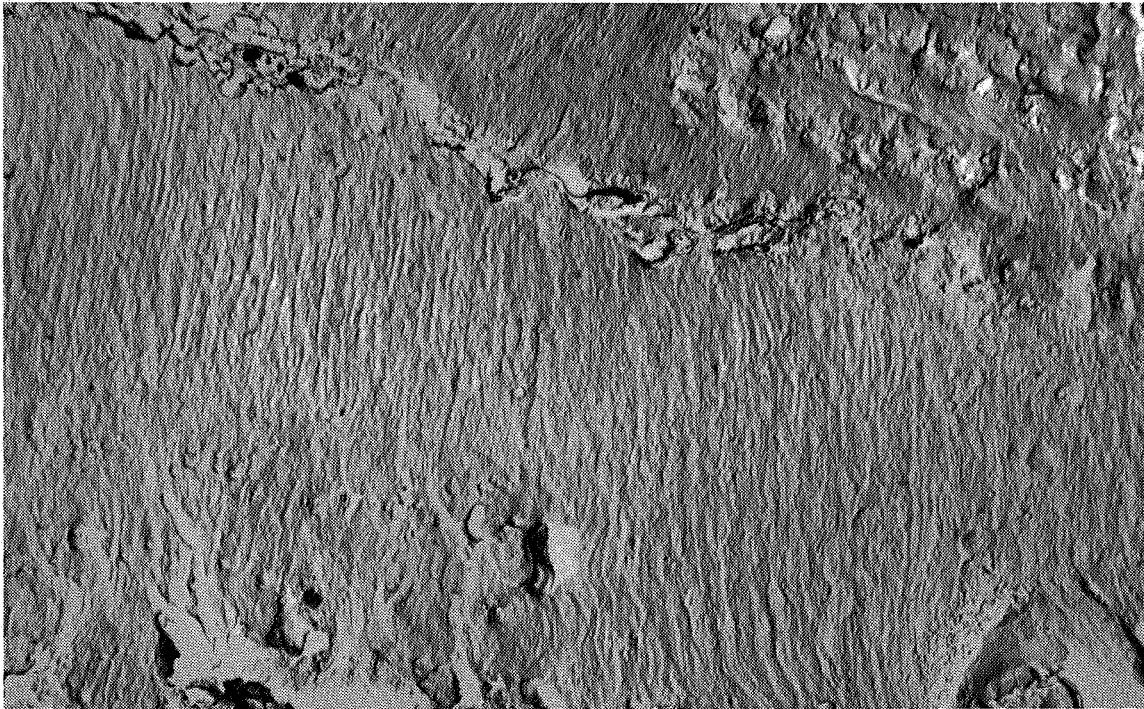
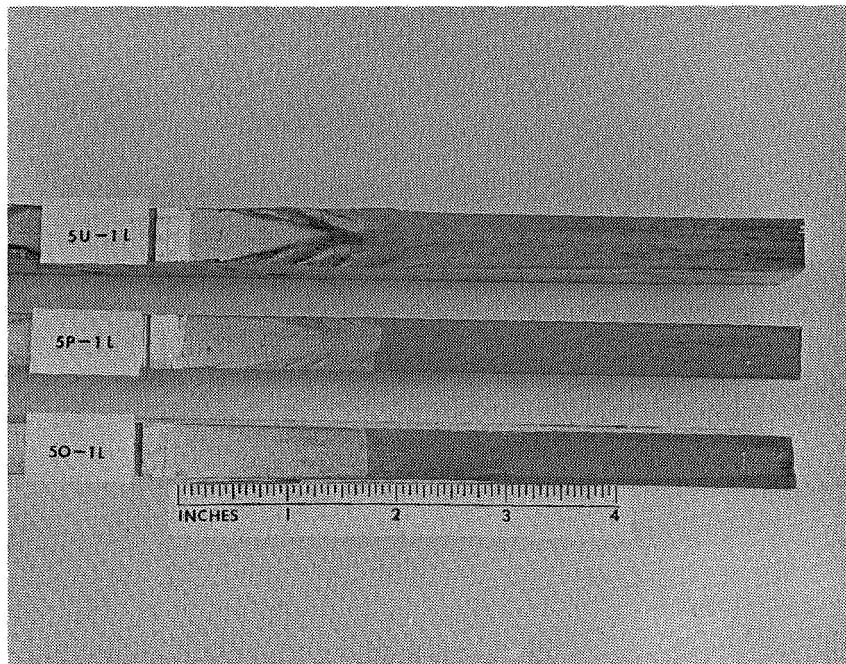
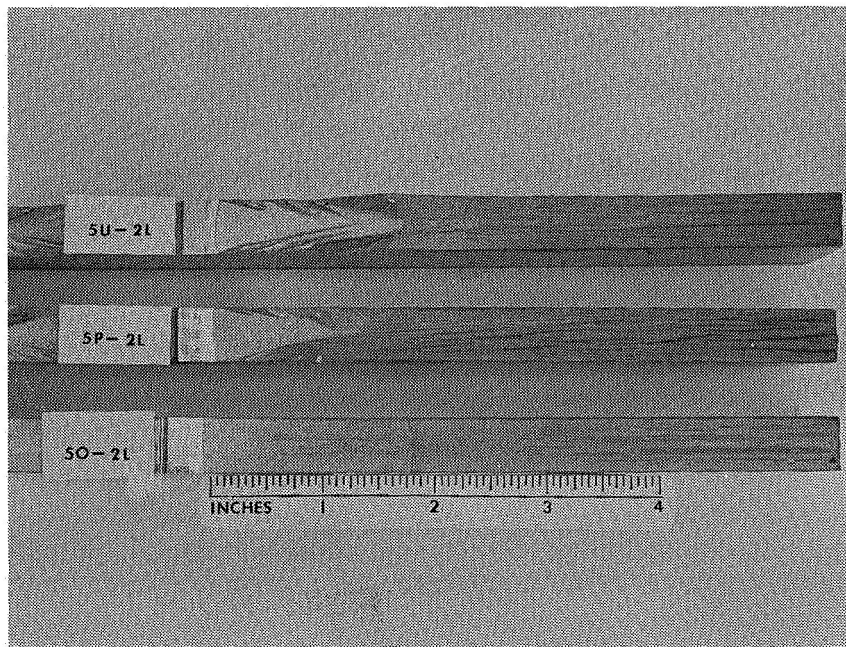


Figure 29. Electron fractographic example of 0.25-inch-thick underaged material tested at -65°F ; $R = 0.05$, $2a = 1.2$ inches (Magnification 3200X)

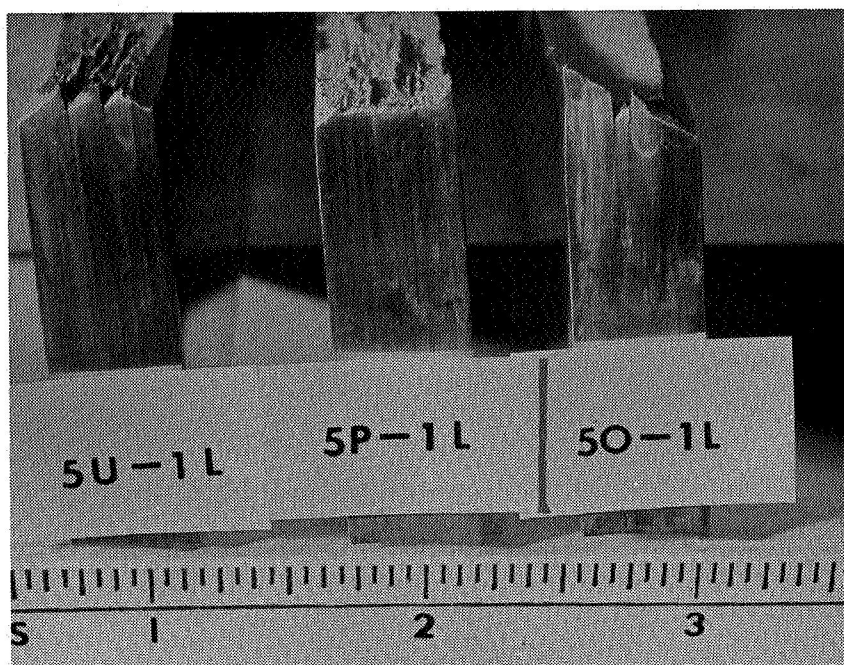


(a) Room temperature in dry air

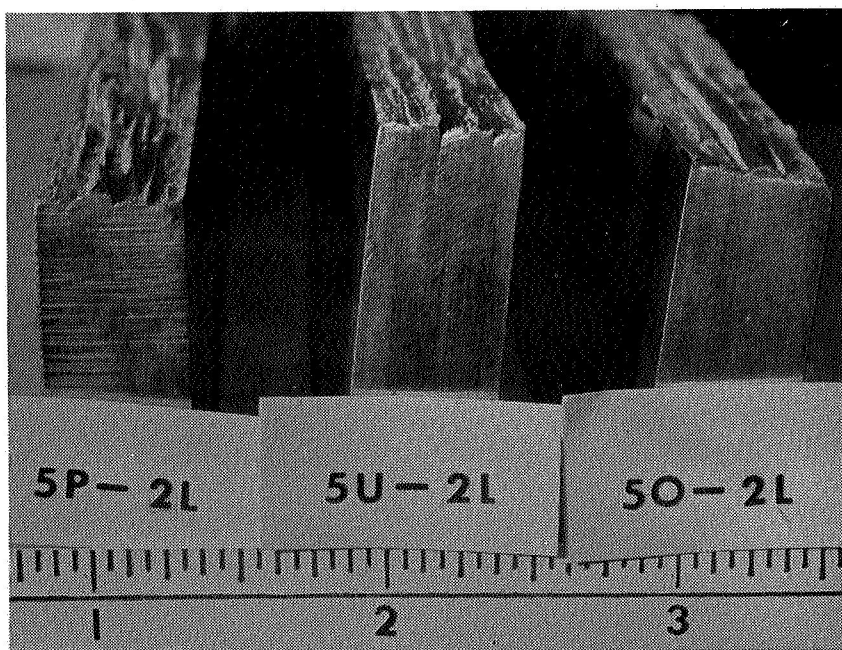


(b) Temperature of -65°F

Figure 30. Macroscopic view 0.50-inch-thick center-notched panels tested at room temperature in dry air, and at -65°F

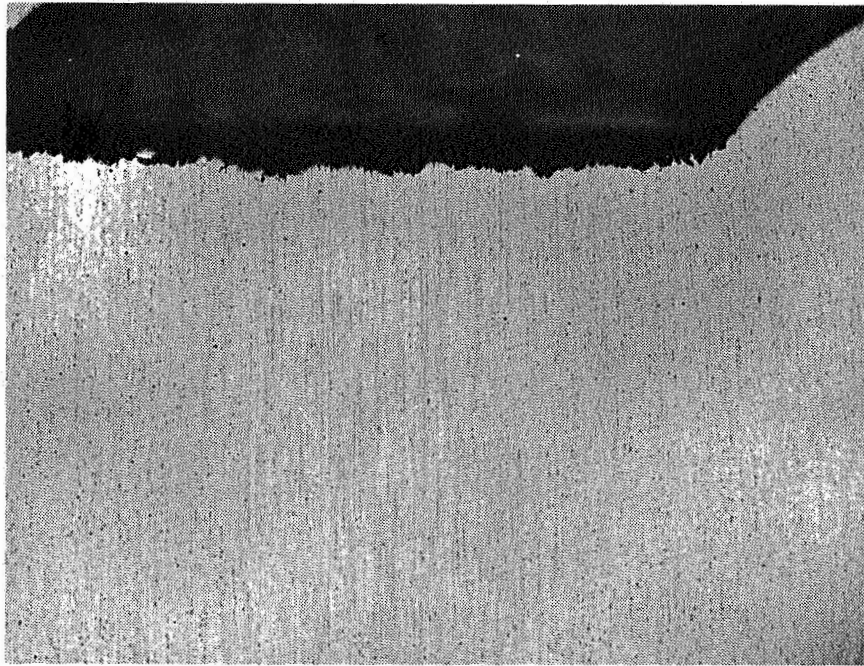


(a) Room temperature in dry air

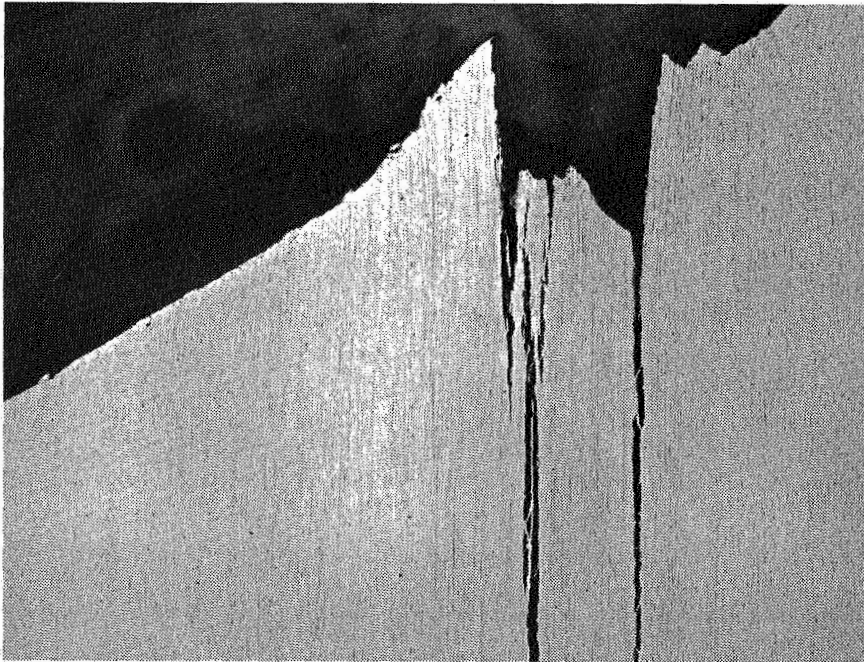


(b) Temperature at -65°F

Figure 31. Macroscopic view of the delamination present at edge of the fracture panels after test at room temperature in dry air and at -65°F

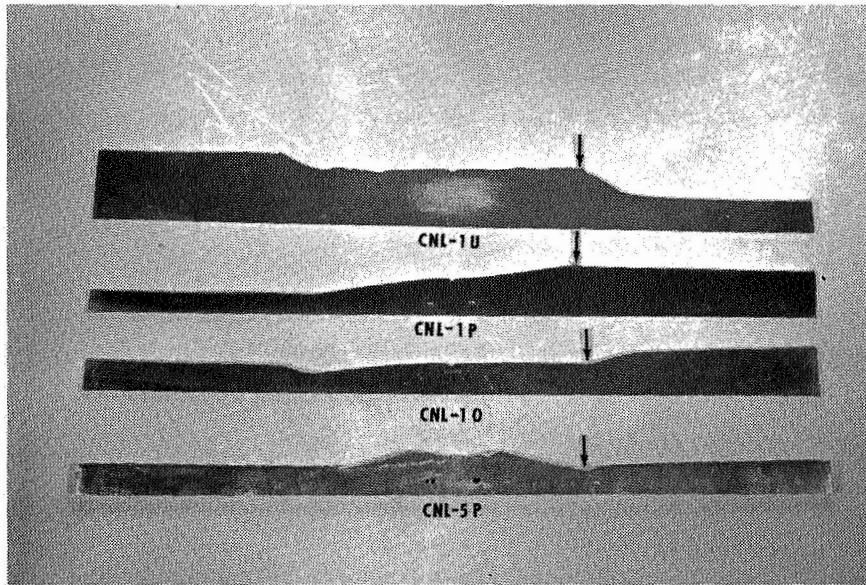


(a) Overaged specimen tested at room temperature



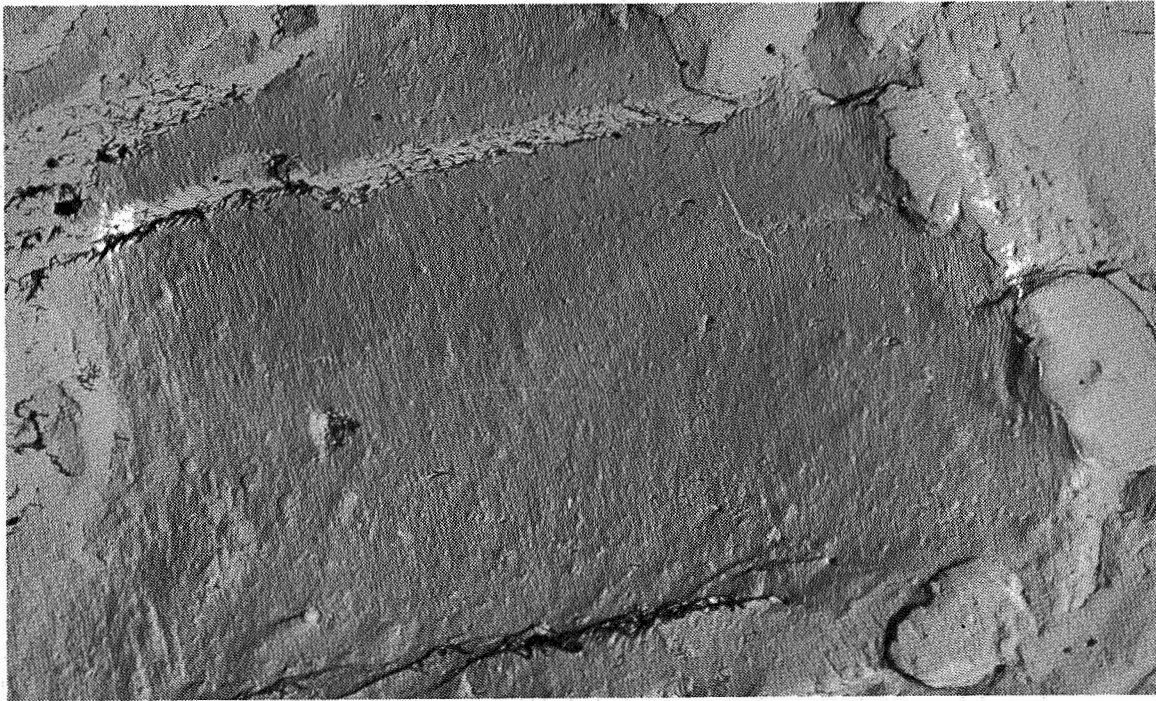
(b) Underaged specimen tested at -65° F

Figure 32. Fracture profile 1 inch from the edge of fracture panels (Magnification 100X)

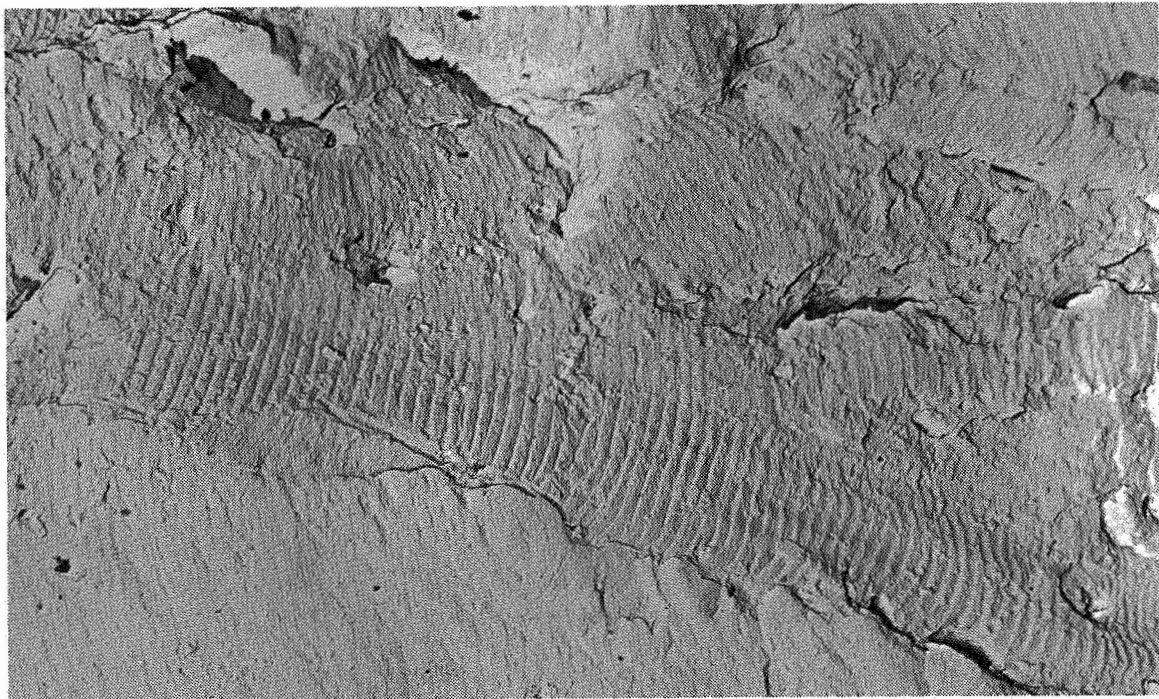


NOTE: Arrows indicate the extent of the fatigue zone

Figure 33. Macroscopic fracture profiles of center-notched 36-inch-wide panels (Magnification approximately 1/10X)



(a) Material 0.160-inch thick



(b) Material 0.500-inch thick

Figure 34. *Electron fractographic comparison of striation spacings under identical test conditions, $2a = 1.0$ inch (Magnification 3200 X)*

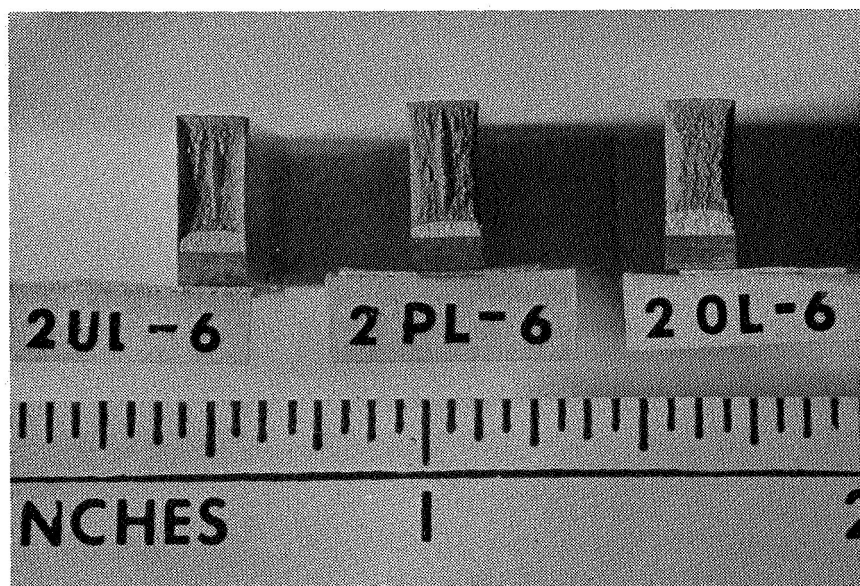
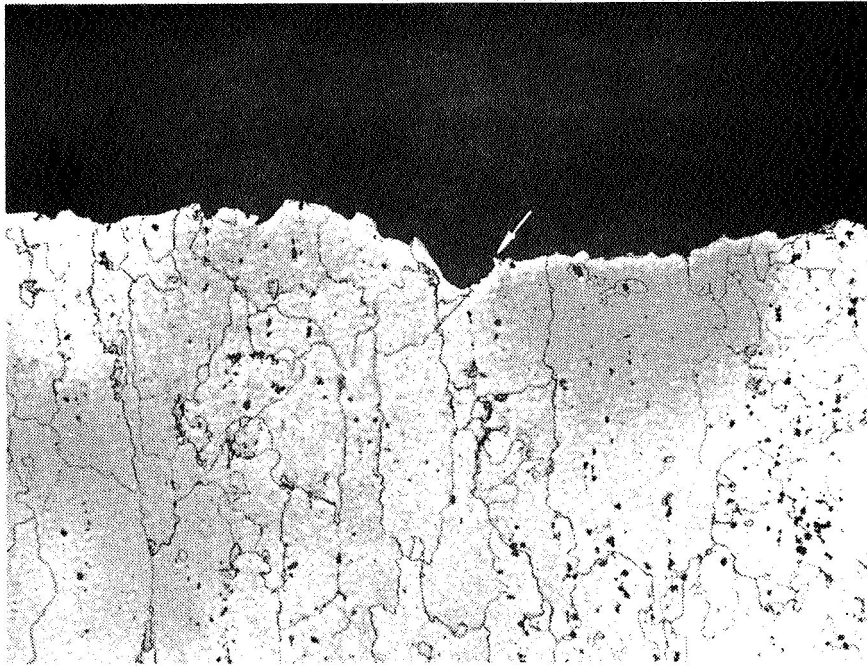
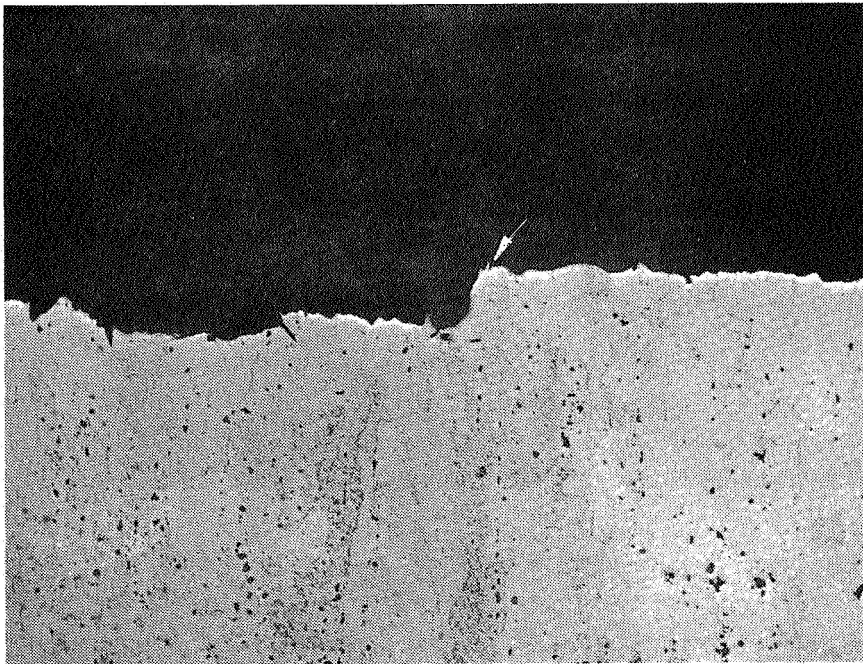


Figure 35. Macroscopic view of the fracture surface of precracked Charpy specimens



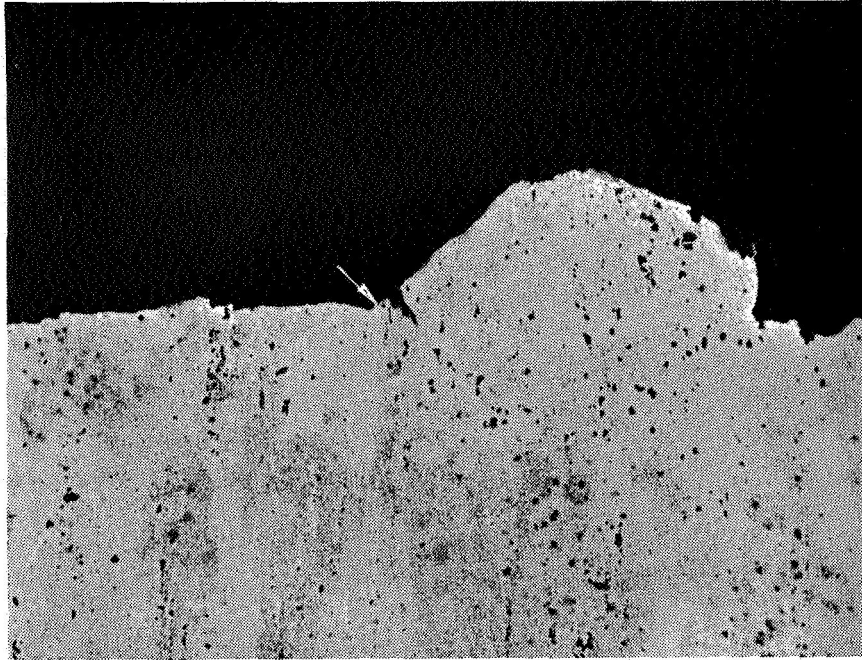
(a) Underaged



(b) Peak aged (T6)

NOTE: Arrow indicates interface between fatigue and fast fracture

Figure 36. Fracture profile through precracked Charpy specimens (Magnification 100X)



NOTE: Arrow indicates interface between fatigue and fast fracture

Figure 37. Fracture profile through overaged precracked Charpy specimens (Magnification 100X)